Diffuse emission of organic trace gases from the flank and crater of a quiescent active volcano (Vulcano, Aeolian Islands, Italy)

Florian M. Schwandner,[1] Terry M. Seward,[1] Andrew P. Gize,[2] P. Anthony Hall,[3] and Volker J. Dietrich[1]

Received 19 June 2003; revised 5 December 2003; accepted 22 December 2003; published 18 February 2004.

[1] Volcanoes discharge a range of inorganic major gas species (e.g., H_2O, CO_2, SO_2, and CO) not only during eruptions but also during quiescent phases through fumarolic and diffuse degassing in their craters and on their flanks. The emission of organic trace gases from volcanoes is similarly not expected to be restricted to discrete fumarolic gas discharges alone. To test this hypothesis, we have sampled soil gas emissions for organic compounds and determined CO_2 fluxes along a profile extending from the vegetated base of the active La Fossa cone (Vulcano Island, Italy) over the unvegetated volcanic flank and up into the crater rim and base and then continuing over fumarolic areas. The results indicate that the majority of volatile organic compounds in the soil gas show significant increases in concentration toward the crater and fumaroles and that diffuse emissions contribute significantly to the volcanic halocarbon source strength. Emissions of the halocarbon CFC-11 (CCl_3F) correlate well with soil CO_2 fluxes measured on site ($R^2 = 0.89$, slope = 1.42 ± 0.1) and both increase toward the crater and fumaroles. Other ozone-depleting substances were found in concentrations significantly above those found in field and system blanks, including CH_3Br, CH_3Cl, CH_3I, C_2H_5Br, and chlorinated benzenes. Abundances ranged from upper pptv to ppmv; for example, the maximum observed CFC-11 concentrations were 1200 pptv in diffuse emissions and 3700 pptv in dry fumarolic gas (average dry air is 268 pptv). On the basis of these results the natural volcanic source strength of halocarbon emissions to the atmosphere requires reevaluation, and in some cases, correction to higher values. Global average fumarolic and diffuse halocarbon source strengths were estimated and scaled to known global volcanic fumarolic and diffuse CO_2 flux data. Among these were CFC-11 ($8.56 \pm 4.7 \times 10^{-6}$ Tg y^{-1}), CH_3Br ($0.98 \pm 0.47 \times 10^{-6}$ Tg y^{-1}), $CHCl_3$ ($94.9 \pm 27.6 \times 10^{-6}$ Tg y^{-1}), and CCl_4 ($3.41 \pm 1.0 \times 10^{-6}$ Tg y^{-1}). *INDEX TERMS:* 0322 Atmospheric Composition and Structure: Constituent sources and sinks; 0325 Atmospheric Composition and Structure: Evolution of the atmosphere; 0370 Atmospheric Composition and Structure: Volcanic effects (8409); 1055 Geochemistry: Organic geochemistry; 8424 Volcanology: Hydrothermal systems (8135); *KEYWORDS:* volcanic gases, halocarbons, natural sources

Citation: Schwandner, F. M., T. M. Seward, A. P. Gize, P. A. Hall, and V. J. Dietrich (2004), Diffuse emission of organic trace gases from the flank and crater of a quiescent active volcano (Vulcano, Aeolian Islands, Italy), *J. Geophys. Res.*, *109*, D04301, doi:10.1029/2003JD003890.

1. Introduction

[2] Since the diminution of the Earth's ozone layer by the increased emission of anthropogenic halogenated organic ozone depleting substances (ODS) became evident in theory and observation [*Molina and Rowland*, 1974; *Farman et al.*, 1985], a large number of studies have addressed the question of a natural contribution to global ODS emissions that may be responsible for a preindustrial constant background burden previously unaccounted for in atmospheric growth models [e.g., *Isidorov*, 1990; *Gribble*, 1994, 1996, 2000; *Butler et al.*, 1998; *Khalil et al.*, 1999; *Reeves*, 2003]. A range of inorganic and organic natural sources has been identified. Among the most prominent inorganic natural sources are sea-salt aerosol [*Keene et al.*, 1999; *Reeves*, 2003], volcanism [*Wilkniss et al.*, 1975; *Rasmussen et al.*, 1980; *Isidorov et al.*, 1990; *Wahrenberger et al.*, 1996; *Jordan et al.*, 2000; *Schwandner et al.*, 2000, 2001a], the oxidation of soil organic matter [*Keppler et al.*, 2000] and crustal degassing [*Harnisch et al.*, 2000]. Organic sources include biomass burning [*Lobert et al.*, 1999], fungal metabolic activity [*Khalil et al.*, 1999], and processes in soils [*Khalil et al.*, 1999].

[3] In the recent decade, international research efforts on halogenated organic ODS have shifted somewhat toward

[1] Institute of Mineralogy and Petrography (IMP), Swiss Federal Institute of Technology (ETH) Zürich, Zürich, Switzerland.
[2] Department of Geological Sciences, University of Manchester, Manchester, UK.
[3] Hall Analytical Ltd., Manchester, UK.

0148-0227/04/2003JD003890$09.00

brominated and iodinated compounds, due to their stronger ozone depletion potentials relative to some chlorofluorocarbons (CFCs) and chlorocarbons. For brominated compounds, methyl bromide (CH_3Br) is the major carrier of atmospheric bromine, with natural sources currently accounting for up to 46% [*Reeves and Penkett*, 1993; *Reeves*, 2003] of the total atmospheric bromine burden. The atmospheric budget of natural CH_3Br sources is still not well constrained [*Butler*, 2000; *Reeves*, 2003], and some sources may still be unidentified. However, new natural sources have recently been identified which include emissions from coastal salt marshes [*Rhew et al.*, 2000], abiogenic production in soils [*Keppler et al.*, 2000], and noneruptive quiescent volcanic emissions [*Wahrenberger et al.*, 1996, 1998; *Schwandner et al.*, 2000]. The natural sources of brominated compounds have been reviewed recently by *Gribble* [1999, 2000] and *Butler* [2000]. For natural thermal sources of halogenated volatile organic compounds, biomass burning is responsible for a significant fraction of global emissions of reactive chlorine [*Keene et al.*, 1999]. Since about 90% of vegetation fires are currently induced by human activity, it is thus considered an anthropogenic source [*Keene et al.*, 1999].

[4] Volcanic gaseous emissions of halocarbons have similarly been interpreted by most authors to date as the product of pyrolysis of adjacent vegetation [*Gerlach*, 1980; *Lobert et al.*, 1999] or alternatively, air contamination [*Gaffney*, 1995; *Jordan et al.*, 2000]. In contrast, organic geochemical evidence indicates a pristine abiogenic origin by high-temperature gas-phase radical reactions [*Schwandner et al.*, 2001b]. For example, the formation of methyl chloride in volcanic emissions of Kilauea (Hawaii) by pyrolysis has been in some doubt on the basis of a comparison of CH_3Cl/CO_2 ratios found in volcanic gases with the products of pyrolysis experiments and biomass burning emissions [*Rasmussen et al.*, 1980].

[5] Chemical variations of volcanic gas emissions are of great complexity. In biomass burning, flaming and smoldering stages of vegetation fires differ greatly in their emissions of pollutants and in the associated processes acting during combustion [*Lobert and Warnatz*, 1993]. In subaerial volcanic emissions, a similar distinction can be made between different types of degassing activity: Violent episodic explosive eruptions, lasting hours to days, and being capable of penetrating the tropopause, and continuous quiescent degassing periods of fumarolic activity, lasting hundreds to tens of thousands of years between major eruptions. These two types of volcanic degassing activity also show chemically distinct patterns. However, true volcanic flames associated with combustion processes are a rare phenomenon and are either due to burning of vegetation buried by lava flows [*Bunsen*, 1847, 1852], self-ignition of sulfur in high-temperature fumarolic fields [*Harris et al.*, 2000], or hydrogen gas burning [*Cruikshank et al.*, 1973; *Naughton*, 1973]. Volcanic hot degassing activity should not be confused with combustion processes.

[6] In this study, we have carried out a field survey to address the question of the origin of halocarbons and other organic compounds emitted from the crater and partially vegetated flanks of a quiescently degassing active volcano. As a test site, we chose the La Fossa cone of Vulcano (Italy), an andesitic volcanic complex that had its last explosive eruption in the late 1880s [*Mercalli and Silvestri*, 1891] and a rejuvenation of unrest a hundred years later [e.g., *Tedesco et al.*, 1995]. The island of Vulcano is one of the most extensively studied volcanoes in the world [*Giggenbach et al.*, 2001] and has a long record of diffuse CO_2 flank degassing measurements [e.g., *Chiodini et al.*, 1998], making it the ideal test site to investigate the origin of halocarbons observed in its fumarolic and diffuse emissions.

2. Experiment

2.1. Sample Collection

[7] The site profile for soil degassing measurements extended from the lower flanks of the volcanic edifice up to and into the crater and was chosen by the following criteria: (1) the profile intersected areas that are vegetated on the lower flanks of the volcanic cone, (2) it is representative of the entire cone from a geological point of view in terms of known subsurface structures and the soil substrate, (3) it does not intersect with active fumarolic vents before reaching the crater, (4) supporting geophysical data are available [*Gex*, 1992], and (5) previous diffuse CO_2 measurements of specific parts of the area are available [*Chiodini et al.*, 1996]. Figure 1 shows the sampling sites as well as the two fumarolic emission points included in this study. Note that the term "soil" may be misleading because the unvegetated surface of the volcanic cone is by and large made up of unstable, coarse, granular rock material (lapilli and ash) of the 1880 eruption that has never supported any visible vegetation.

[8] Soil gas CO_2 emissions were determined using the dynamic chamber method [e.g., *Chiodini et al.*, 1998] with CO_2 being measured with a portable IR-Sensor calibrated to CO_2 (Multiwarn II®, Dräger GmbH, Kiel, Germany). All sampling sites except number 13 yielded data in the linear range of calibration for the CO_2 sensor. In order to calculate diffuse soil mass fluxes by the dynamic chamber method, the sensor readings have to be corrected for air pressure and temperature, assuming ideal gas behavior. Temperatures were measured using an Inconel sheathed K-type thermocouple that was inserted along a glass sampling tube into the ground and was carefully sealed where it intersected the surface. The air pressure [kPa] was measured using a simple barometric altimeter (Casio 1160 DW-6500-1V) that was calibrated daily against mean local sea level (precision 1%). The site temperatures were also measured in air (10 cm above ground, shaded) and at the soil surface 0.5 cm beneath the surface as well as in the shallow soil at 1 cm intervals to varying depth. These measurements yielded soil temperature gradients as auxiliary data (see Figure 2).

[9] Figure 3 displays a schematic of the sampling setup. The organic trace gases were sampled using an active adsorbent tube technique which was a customized version of U.S. EPA method SOP 2042 (Figure 3). A two-piece stainless steel probe was inserted into the ground to about 0.6 m depth, its solid central rod removed and replaced by a glass tube (1 m length, 4 cm diameter, lower end perforated) and then finally, the outer steel jacket tube pulled out so that only the glass tube remained. The top of the glass tube was connected to a custom made conical-convex glass reducing union to 6 mm OD. This connection was further stabilized with a piece of wide-bore silicone rubber hosing that did not

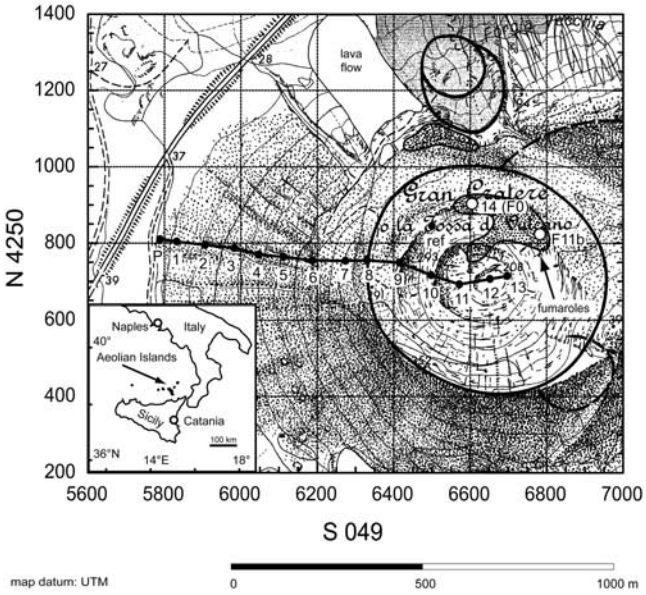

Figure 1. Map display of the La Fossa volcanic cone on Vulcano (Aeolian Islands, Italy), modified after *Keller* [1970], showing the sampling sites. The stippled field displays the approximate location of the area of fumarolic activity, and the solid areas are lava flows. Thick lines indicate crater outlines, and the open circles show the locations of the fumaroles described elsewhere (F. Schwandner et al., manuscript in preparation, 2004), of which site 14 (fumarole F0) is included in this study. Point "ref" is a geodetic reference point.

come into contact with the sampled gas. A Swagelock® brass union with Supelco M4 ceramic/graphite composite ferrules (Supelco Inc., PA, USA) was used to connect the sampling tube (adsorbent cartridge) to the reducing union. This connection was demonstrated to be airtight, and did not permit air entrainment. It was additionally used for fumarole sampling, where samples in cold-sealing copper tubes were taken using this setup for noble gas isotope analysis. The results show that the maximum air fraction entrained in this type of sampling setup is significantly less than 10^{-5} (<0.00035%).

[10] A battery-driven, low-flow pump was connected to the sampling cartridge on its downstream end by the same type of Swagelock® union, a piece of 6 mm OD glass tubing, and a piece of 5 mm ID silicone hose. The pump's wetted surfaces were Teflon coated and the pump exhaust was collected in Tedlar® bags to avoid any backflow of air. The pump was a calibrated SKC 222 Series Low-Flow Sample Pump (SKC Inc., PA, USA), set to a flow rate of approximately 80 mL/min. This yielded approximately 1.5 L of gas per sample. Prior to sampling, the air contained in the sampling train was carefully purged to allow slow admixing of soil gas but to avoid air entrainment. The pumped volume was calculated from (1) the collected volume in the Tedlar® bag, (2) the flow rate and sampling time, and (3) the number of strokes and the calibrated stroke volume against a similar resistance.

[11] The adsorbent cartridges (SKC Inc., PA, USA) contained three adsorbent beds consisting of Carbotrap C, Anasorb CSC, and Carboxen 569. Presampling conditioning of the cartridges was done under a stream of purified helium (grade 5) at 300°C with in-line oxygen and hydrocarbon traps. During sampling, they were cooled by ice packs and wrapped in aluminum foil to avoid possible photolysis of analytes by sunlight. After collection, the cartridge ends were immediately capped by standard end caps (Kapak®) that are specifically designed for that purpose in air monitoring (SKC Inc., PA, USA). Storage prior to analysis was at −18°C. Sampling of the fumarolic volcanic gases follows a different protocol that is detailed elsewhere [*Schwandner et al.*, 2001a].

[12] *Couch et al.* [2000] used an alternative method that involved the sampling of a portion of soil into containers. The advantage of our method is that transport and storage of sealed adsorbent cartridges is much easier and avoids contamination problems encountered with soil samples. Furthermore, the decomposition and reaction of compounds during transport and storage of soil material may be a problem given the complex substrate of an actual soil sample, including the microorganisms contained. It also precludes a meaningful soil gas analysis due to significant air entrainment, as opposed to in situ sampling methods such as the one employed in this study.

2.2. Analytical Methods

[13] The adsorbent cartridges were thermally desorbed at 300°C under a stream of purified helium, readsorbed onto a PDMS/Carboxen (PDMS = polydimethylsiloxane) coated SPME fiber (Solid Phase Microextraction, Supelco Inc., USA) at constant temperature (25°C) and then thermally desorbed in the inlet system (splitless) of the gas chromatograph (GC). The separated eluents were analyzed by full-scan single quadrupole mass spectrometry (MS). To release the adsorbates from the adsorbents, we used a simple custom-built short-path thermal desorption purge-and trap system, optimized to minimize sample loss and fractionation of analytes (Hall Analytical Ltd., UK), with external temperature control, flow control and all-glass contact surfaces [*Schwandner et al.*, 2001a]. The same high-purity helium supply was used for desorption as in the conditioning of the

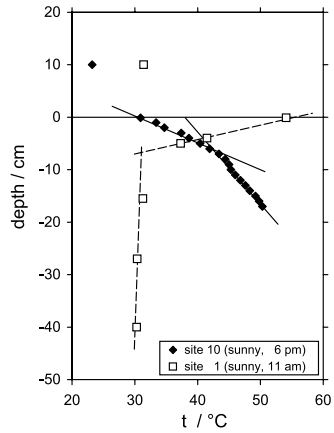

Figure 2. Temperature-depth graph of two sampling sites at the base of the cone flank (site 1) and within the crater (site 10). Both measurements show a clear distinction between the linear insolation and the geothermal gradients.

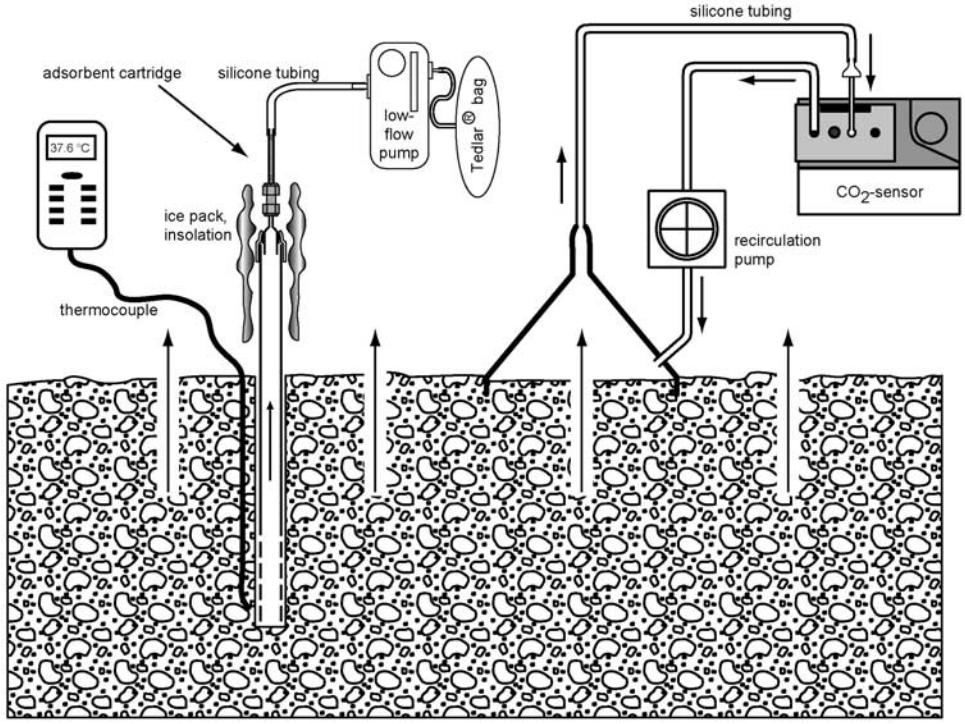

Figure 3. Schematic diagram of the sampling setup for diffuse soil gas sampling (left) and CO_2 flux measurements.

adsorbent tubes. A simple custom-built cryocooling device concentrated the analytes at the head of the analytical column in order to ensure a low baseline. The analytical column was a dedicated 100% cross-linked low-polarity PDMS fused-silica Hall-GC1 analytical column (equivalent to the stationary phase OV-1) with the dimensions 60m length, 0.32mm inner diameter, and 0.5 μm film thickness (Hall Analytical Ltd., UK). Using in-line filtered helium 5.0 as a carrier gas, the column head pressure was 8 psi (flow rate of 0.54 mL/min, average linear velocity of 18.8 cm/s) with a theoretical helium holdup time of 5 minutes and 32 seconds. The phase ration β was determined as 160. The oven was run in a temperature program of 8 min isothermal (40°C), 4°C/min ramp to 290°C, and then isothermal again for 17 min at the final temperature.

[14] The analyses were performed on two different GC-MS systems: A Thermoquest Voyager GC-MS system coupling a Fisons GC 8060 with a Thermoquest Voyager MD 800 single quadrupole mass spectrometer and an HP GC 5890A coupled with a Micromass Trio-2000 single quadrupole mass spectrometer. The latter was used on one sample from a vegetated site at the base of the volcanic cone to determine target compounds and retention indices at higher resolution than in the routine analyses of all sampling sites as well as for analysis of a field blank (unused cartridge). The acquisition software used was MassLab 1.3 and VG MassLynx 3.0 for NT, for the MD 800 and Trio-2000 instruments, respectively. Both MS systems were operated in electron impact mode (EI+) at 70 eV electron current, and a scan rate of 1 scan per second. Mass ranges were 15–600 a.m.u for the MD 800, and 20–549 a.m.u. for the Trio 2000. The transfer line was kept at 300°C, connected in both cases to the GC column end by a capillary open split connection. Sufficient system, SPME needle and column blanks were analyzed in between sample runs to ensure purity of the process, including also a field blank of identical adsorbent tubes analyzed under identical conditions and ambient and laboratory air blanks. Instrumental drift on the detector response was monitored daily by an internal standard leaked into the mass spectrometer, and the mass spectrometric conditions (i.e., repeller energy) were optimized accordingly (which was rarely necessary). The instrument was entirely dedicated to this study, operated under the same conditions permanently (also nights and weekends) and no replacement of filament or ion source was undertaken. The stability of the sensitivity was within a 5% margin (maximum) in day-to-day operation. Over the entire period of time during which the analyses were made, the total maximum variance between the measurements as a group was no more than 10%. This long-term variance maximum was reduced by the daily use of instrumental standards and the periodic use of external standards. Given the low detection limits (around 100 pptv) for this strongly adverse sample matrix (strongly acidic, hydrous and sulphurous, unlike typical air samples), an analytical precision of around 5% is better than typical precisions for similar types of measurements (e.g., incinerator stack gases) and represents one accomplishment of this study.

[15] The raw data were analyzed by indexing all compounds relative to *n*-alkane and separately to *n*-aldehyde homologues, and then performing a scan-by-scan mass fragment analysis of the compounds. Natural *n*-aldehyde retention indices are easier to target in samples of soil gases influenced by vegetation than *n*-alkanes and were used as secondary confirmation. For a number of compounds, molecular ion peaks were preserved and indicated approx-

imate molecular masses of compounds. Library spectra were used as suggestions and were considered indicative of a compound's identity. Retention indices served as targeting help for specific compounds, such as isomer identification and in some cases, as confirmation for mass spectral identifications.

[16] The method previously developed by us and applied in this work was shown to be unaffected by contamination (air entrainment, carryover/memory, or instrumental sources such as glues, seals and washers) during analysis (Figure 4). In Figure 4, diagrams A through E represent a typical temporal analytical succession of a sample with preceding and succeeding analytical blank runs. In this example, the retention window for chloroform ($CHCl_3$) is shown, derived from literature data of chloroform retention data on the same stationary phase (DB-1). The chromatograms are reconstructed ion chromatograms (RIC) of mass/charge ratios (m/z) 83 and 85 (indicative of chloroform) from acquired GC-MS data. The errors 1 and 2 define the retention window and represent the standard error from multiple slightly deviating literature values of retention indices, $\mathbf{I_{R}}_{lit}$, for chloroform (error 1), and the same deviation applied to the lowest and highest reported $\mathbf{I_{R}}_{lit}$, respectively (error 2). Diagrams A and B are the first and second (last) analytical blanks before the sample (C) is analyzed; no carryover or contamination is evident for the peaks of interest (The diagrams A and B are 1495 times enlarged with respect to C, as are D2 and E). Diagram C is the volcanic gas profile end-member sample also represented in later figures. Diagram D1 is the first analytical blank (method run of analytical system without sample) after the sample run shown in C, at the same vertical scale as C: Small memory peaks can be seen, in the case of chloroform representing at most 0.6% of the integrated peak area of the sample run (C) and documenting a superb recovery for this compound. Diagram D2 is the same plot as D1, but at the same enlarged scales (1495 times, relative to C and D1). Diagram E represents a second analytical blank after D, showing the complete removal of memory peaks prior to the next sample analysis.

[17] Table 1 lists a selection of compounds discussed in this study together with data and information relating to the uncertainty in calibration, field blank readings, and concentration ranges. The further treatment of the raw data after peak identifications included manual and automated peak area integration, a correction factor for the sampled gas volume, determination of concentrations by means of a calibration function (see Table 1) and field blank subtraction. Analytical system blanks were always repeated until the background was sufficiently low (see Figure 4) such that no additional correction was necessary. Instrumental drift was determined on a daily basis and led to only negligible corrections (see above). Standardization was performed by charging several adsorbent tubes with different known amounts of a certified standard gas (TO-14 series compounds, Scotty Inc., NL). It was not known prior to this study what organic compounds could be expected in diffuse emissions on volcanoes. We therefore chose to use a screening standard targeted to halocarbons (TO-14) as a reference material. As a result, not all compounds found and reported in this study were quantified. Calibration results and repeat standard analyses gave a precision of better or equal to 2% for most compounds considered in this study (Table 1); R^2 values of the calibration curve from 0.125 ppbv to 12.5 ppbv were better than 0.99 for all compounds except CH_3Cl, benzene (this compound was not quantified with sufficient confidence), CFC-114 (0.90), DCM (0.88), toluene (0.97), chlorobenzene (0.82), and *m*- and *o*-dichlorobenzene (both 0.96). Styrene was included in the list of compounds because its concentration variations are significantly larger than the error, despite a poor calibration (Table 1). The greatest source of error (i.e., contamination) appears to be from compounds present on the desorbed, uncharged, adsorbent cartridges or from laboratory handling, as indicated by the field blank (reported as BLK). In all cases, the contamination from these sources was less than 5% except in the case of benzene and some *n*-alkanes for which the contribution to the sample analyte peak area readings was up to 10%. Here we report quantitative and relative values in order to be able to compare a larger range of compounds and groups with each other and with measured parameters at the various sampling sites.

3. Results

3.1. Site Parameters and CO_2 Flux

[18] To identify the sources and boundary conditions for organic trace gases emanating from an active volcano, an understanding of subsurface structures as well as site conditions is required. The site parameters considered in this study are the precise location and altitude, air pressure, thermal properties of the ground, the diffuse CO_2 flux through the soil, the vegetation distribution, and the conductive heat flow as calculated from the temperature measurements (Figure 2). From the available literature, the apparent ground resistivity [*Gex*, 1992] as well as geological surface and subsurface information was included [*Keller*, 1970, 1980; *Chiodini et al.*, 1996]. The available geological, geochemical and geophysical literature on Vulcano is large and will not be reviewed here. For an introduction, see *Fulignati et al.* [1998]. The results of the physical measurements are displayed in Figure 5.

[19] In the air pressure profile diagram (Figure 5d) it can be seen that expected variations with altitude of over 3 kPa occur systematically throughout the profile, but that the actual topography is not accurately reproduced. The air pressure was measured as a correction factor entering in the calculation of the CO_2 flux from the sensor measurements [*Brombach*, 2000], as specified in the previous section.

[20] The temperature measurements yielded several different trends. Figure 2 shows two representative temperature measurements at two sites in the profile. At both sites the temperature changes linearly with depth with two different slopes that clearly separate the temperature-depth profile into two discrete sections. The upper section trend would be expected to be due to solar heating of the black soil surface (the ''shallow soil insolation(=solar heating) gradient'' in Figure 5b). The second, deeper section at each site is the steady state geothermal gradient (displayed as its directly measured inverse value dz/dt in Figure 5b). In the upper section of site 1 (open squares), solar heating produces the expected signal with a positive slope whereas site 10 displays a negative slope, indicating anomalous

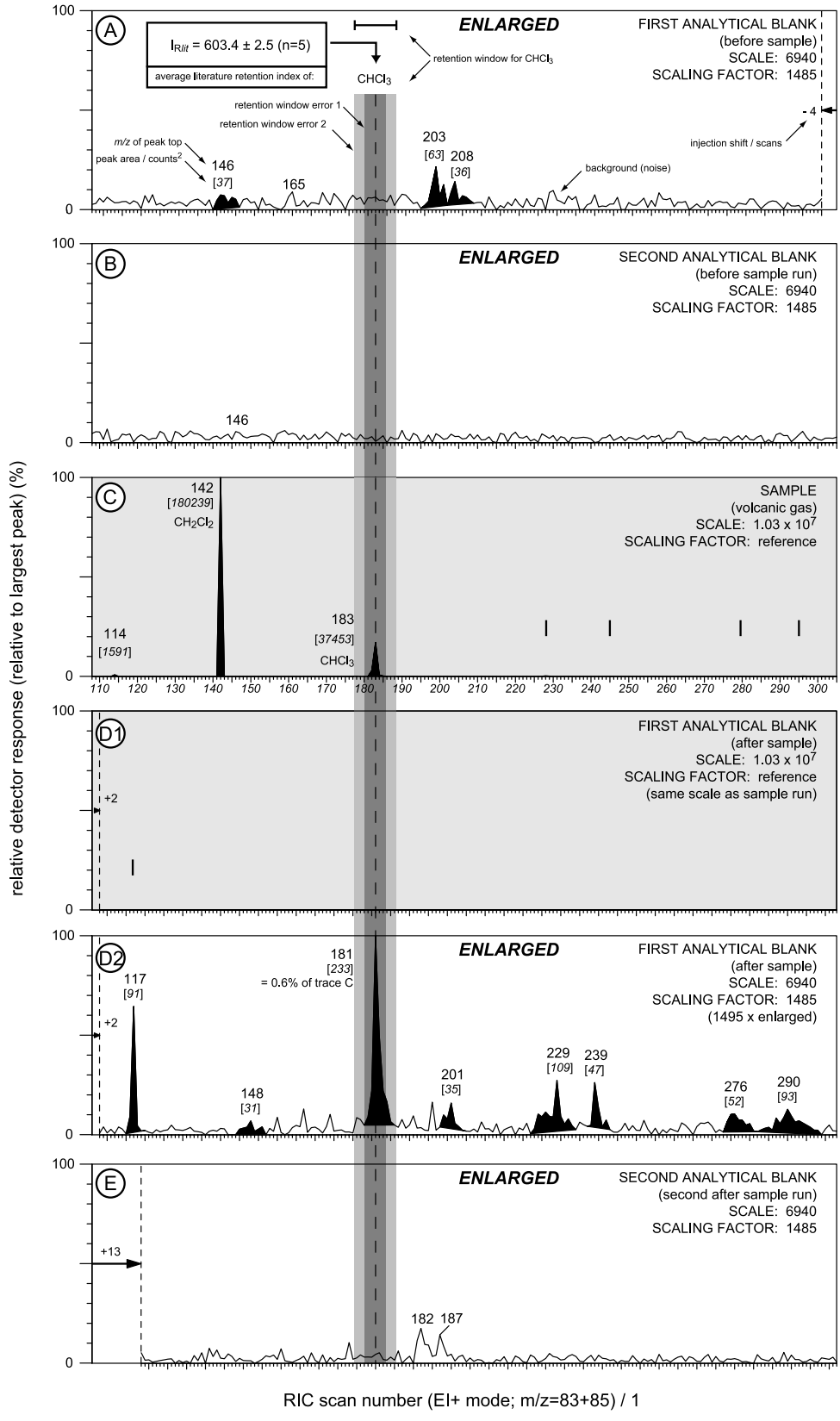

Figure 4. Reconstructed ion chromatograms (RIC) A–E: Acquired intensity versus scan number data for mass/charge ratios (*m*/*z*) 83 and 85; see text for explanation.

Table 1. Quantitative Information on a Selection of Compounds Discussed in This Study[a]

IUPAC name	Quantifier Ions, m/z	Formula	M, g/mol	Figure Number	Field Blank, Percent of maximum	Field Blank, ppbv	Calibration		Concentration Range			
							S_{AC}[b] % (Residuals)	R^2	Minimum, ppbv	Maximum, ppbv	Average, ppbv	n
Methyl iodide	127 + 142	CH_3I	156	6c, 10	10.3	n.q.	n.d.	n.d.	n.q.	n.q.	n.q.	
Methyl bromide	94 + 96	CH_3Br	95	6d, 10	b.d.	b.d.	1.1	1.00	b.q.	5.9 ± 0.1	b.q.	9
Methyl chloride	35 + 50 + 52	CH_3Cl	51	6c, 10	0.1	n.q.	n.d.	n.d.	n.q.	n.q.	n.q.	
Methylene chloride	84 + 86	CH_2Cl_2	85	12	0.9	b.q.	17	0.88	b.q.	767 ± 130	265 ± 45	15
Trichloromethane	47 + 83 + 85 + 87	$CHCl_3$	119	4	b.d.	b.q.	1.8	1.00	16.4 ± 0.3	50.4 ± 0.9	27.5 ± 0.5	9
Tetrachloromethane	117 + 119 + 121	CCl_4	154	10	b.d.	b.d.	3.4	1.00	b.q.	1.7 ± 0.1	b.q.	8
Trichlorofluoromethane	101 + 103	CCl_3F	137	10, 11, 12	0.2	b.d.	2.4	1.00	0.2 ± 0.0	3.6 ± 0.1	0.6 ± 0.0	15
Bromoethane	108 + 110	C_2H_5Br	108	10	0.2	n.q.	n.d.	n.d.	n.q.	n.q.	n.q.	
Chlorobenzene	77 + 112 + 114	C_6H_5Cl	112	10	n.d.	b.q.	22.8	0.83	b.q.	b.q.	b.q.	13
Dichlorobenzene[c]	146 + 148 + 150	$C_6H_4Cl_2$	147	10	11.2	12.5	3.1	0.99	b.q.	237 ± 7	46 ± 1	12
Styrene	63	C_8H_8	104	7	0.1	b.q.	44	0.40	b.q.	2650 ± 1166	359 ± 158	13
C2-substituted arenes[d]	91 + 106	C_8H_{10}	106	7	0.3	10.9	1.19	1.00	b.q.	645 ± 8	182 ± 2	13

[a]Fumarolic source strength, based on average global analyte concentrations in fumarolic emissions (F. Schwandner et al., manuscript in preparation, 2004).
[b]S_{AC} is the residual error of the calibration curve at 12.5 ppbv.
[c]Sum of all 3 isomers.
[d]Sum of all 4 isomers.

warming from depth or surface cooling. In the crater at site 10, the heat released from depth is expected to be greater than at site 1 (at the base of the flank of the volcanic edifice). At site 10 the subsurface heat flow dominates the temperature profile and solar heating is expected to cause only a minor disturbance. The upper section of site 10 is best explained by surface cooling of the shallow soil that is continuously heated by a strong subsurface heat flow despite extensive solar heating after a warm sunny day (measured at 6 pm). Surface cooling merely alters the strong thermal signal of the crater region slightly.

[21] In Figure 5c the temperature of intersection of the shallow soil solar heating gradient and the geothermal gradient are plotted together with the air temperature. The two curves show no relation to each other, indicating that the depth of intersection is not controlled by solar heating but by surface advective cooling and the geothermal gradient. The depth of intersection is also a measure of how strongly the subsurface thermal release penetrates through the soil. Finally, the conductive heat flow, H, was calculated from the thermal data using Fourier's law [*Brombach et al.*, 2001],

$$H = -\lambda \frac{dt}{dz} \tag{1}$$

where λ is the thermal conductivity constant having a value of 1.25 ± 0.25 W m^{-2} $°C^{-1}$ in unconsolidated volcanic sediments [see *Brombach*, 2000], t is the temperature in degrees Celsius and z is depth in meters. The resulting graph in Figure 5 shows, as expected, that the heat flow increases with proximity to areas of fumarolic activity.

[22] The measured CO_2 soil gas flux (Figure 5e) is higher near the crater and is largest at sites where faults are inferred from surface geology and surface degassing structures. At the crater bottom it approaches zero because of decreased permeability due to the underlying magmatic plug and the consolidated character of the accumulated fine epiclastic alluvial volcanic debris that fills the crater bottom. Sites 7 through 12 represent a section of the profile that overlaps with a similar published CO_2 flux profile acquired in 1995 [*Chiodini et al.*, 1996], where the site-to-site variations ("profile shape") of fluxes are qualitatively the same as in our study, however of lesser quantity. CO_2 fluxes at Vulcano are known to quantitatively vary over time [e.g., *Chiodini et al.*, 1998]. The qualitative "profile shape" of degassing data therefore appears to be highly robust.

[23] Similar CO_2 measurements in 1995 resulted in qualitatively similar flux profiles [*Chiodini et al.*, 1996], indicating that the structural and thermal regime has been relatively unchanged over the previous 6 years. The variation of the fluxes along the profile is in its basic features (an increase mid-profile and in the crater region) similar to variations in ground resistivity data obtained along the same profile (Figure 5f) 10 years earlier [*Gex*, 1992]. Two zones of elevated values can be identified within 0 to 200 m profile distance (sites P to 5), and between 550 and 800 m profile extend (sites 8 to 11), with a pronounced low-value "valley" between these two zones, for both parameters. The CO_2 and resistivity profiles suggest active faults and/or active degassing at shallow depth. An increased gas pressure dilates pores and the gas is in itself a poor conductor, leading to an increased resistivity over subsurface degassing

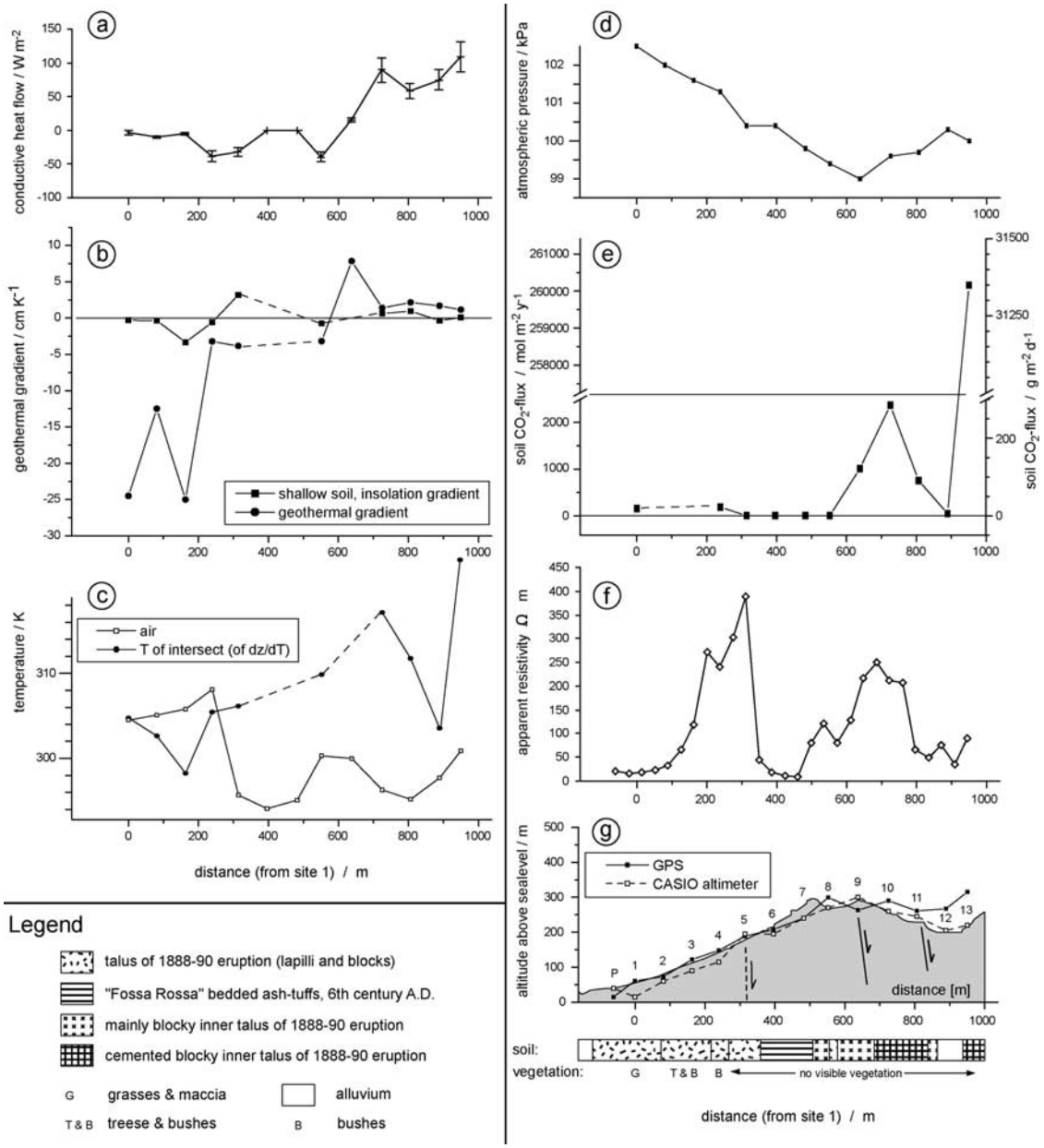

Figure 5. Parameters measured in the field and derived quantities. The abscissa refers to the distance from the first sampling site (i.e., site 1) at the base of the flank of the volcano. In diagrams (a–c), thermal parameters are displayed, in diagrams (d–g), altitude, pressure-corrected CO_2 flux, and atmospheric pressure are shown together with basic botanical, structural and surface geological data. For comparison, literature values of the apparent resistivity along the same profile are also shown [*Gex*, 1992].

features, such as actively degassing subvolcanic magmatic intrusions and/or deep reaching faults.

3.2. Chemical Parameters

[24] A large range of compounds was targeted and identified and only a representative selection is given here. Figures 6–11 display the chemical signals along the measured profile ordered by compound group (Figures 6–8), as the C_7-C_{20}*n*-alkane distribution (Figure 8), and as correlations between selected compounds and physical parameters (Figures 6 and 11). The sites along the profile can be subdivided into four major zones: (1) the vegetated lower flank of the volcano, (2) the barren upper flanks of the volcano facing away from the crater with its hot gas emissions but toward Vulcano town, (3) the barren crater area with obvious diffuse degassing structures, and (4) the fumaroles and fumarolic fields with ground temperatures of 50-100°C and high diffuse CO_2 fluxes. Site 1 is excluded in the diagrams of Figures 6–8 since it was analyzed by higher-resolution GC-MS system in order to obtain reliable retention index information. Site 13 is grouped with the fumaroles because it is situated within the outer area of a fumarolic field, with ground temperatures approaching 100°C and high CO_2 fluxes (see Figure 5). Site 14 is a fumarole (F0) and is slightly off the profile (see Figure 1). The blank analysis reported in Table 1 shows that all

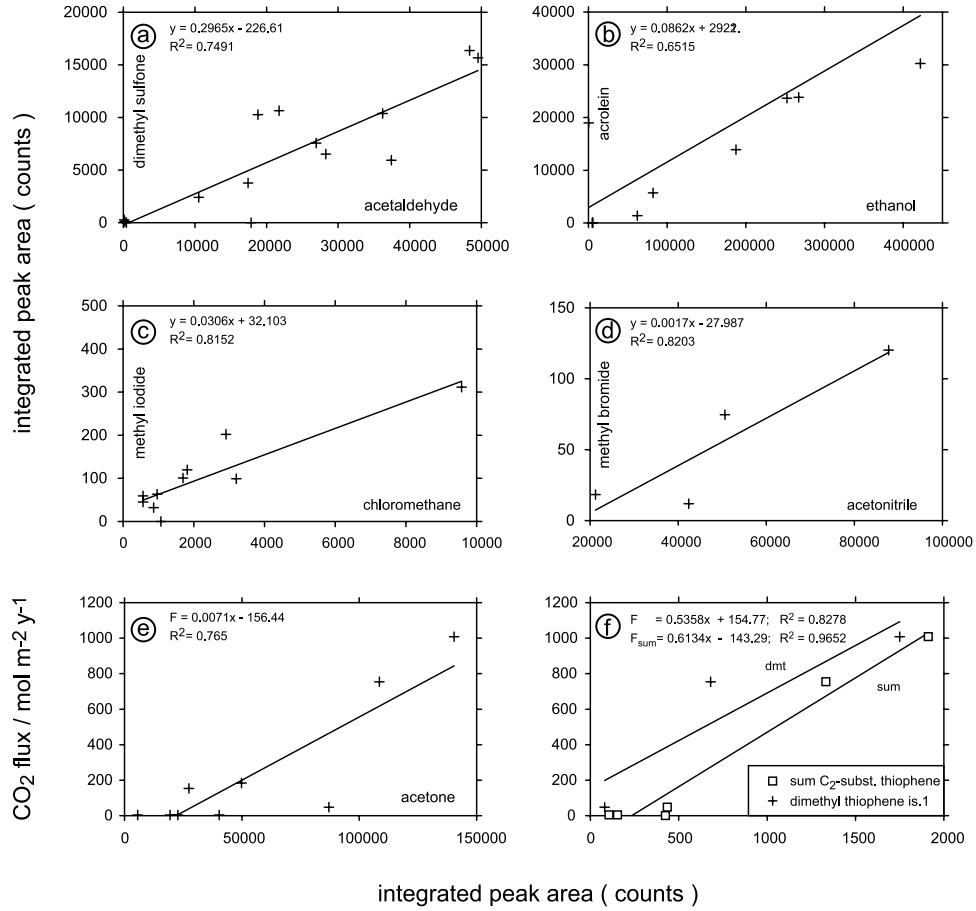

Figure 6. Correlation diagrams of compounds and CO_2 flux (see Figure 11). In all diagrams the abscissa refers to integrated peak areas (sampling volume corrected) of compounds present at various locations through the profile, excluding the fumarole F0 (site 14). In Figures 6a–6d the ordinate displays the integrated peak areas of other compounds in the same samples. In Figures 6e and 6f the ordinate is the measured site CO_2 flux, F (see Figure 11). Correlation parameters are shown for each diagram, as the correlation function derived from linear least squares regression of the data, and the R^2 correlation coefficient. Note that in Figure 6, two data sets are shown: The sum of all C_2-substituted thiophenes and the first eluting dimethyl thiophene isomer. The summed data include the data points represented by the dimethyl thiophene isomer. Instrumental precision was 5% or better.

analytes are significantly enriched, indicating that contamination is negligible even under lengthy, hot and corrosive field sampling conditions where the field blank (i.e., an unused adsorbent cartridge) was carried along at all times.

[25] The greatest blank contamination was detected for thiophene, reflecting the extremely low abundance in the vegetated zone of the profile (see Figure 9), where it was only detected in the site 1 sample because of the use of a higher-resolution MS in analysis. Consequently, contamination is lower by up to an order of magnitude in samples that have a higher concentration (i.e., in the crater area). The lowest contamination is found for halocarbons, nitriles and arenes. In a number of cases, compounds were not detected in the blank at all. This shows that contamination can be safely ruled out as a source for these compounds. Air contamination during sample collection was observed to be minimal using the techniques employed as indicated by measurements of noble gas isotopes and inorganic atmospheric gases (F. Schwandner et al., manuscript in preparation, 2004).

[26] Before discussing the individual compound groups, the figures are introduced as follows. In Figures 7, 9, and 10 a range of representative compounds are displayed in abundance versus "profile distance" graphs, ordered by compound groups. The profile distance is measured relative to the starting point at the base of the profile on the vegetated lower flank of the volcano (site 1). In these diagrams, enrichments can be directly read for individual compounds at certain sites or zones along the profile. For clarity of comparison, the integrated peak areas, A_i, for a given compound found in the profile, are displayed relative to the largest integrated peak area found in the same sample set, A_{max}, in percent. The quantity, y, is the compound abundance obtained after correcting for sampling volume (equation (2)):

$$y = \frac{m_i}{m_{\max}} \times 100. \tag{2}$$

[27] This expression is mathematically the same as when calibrated concentrations were used because the slope, z, of

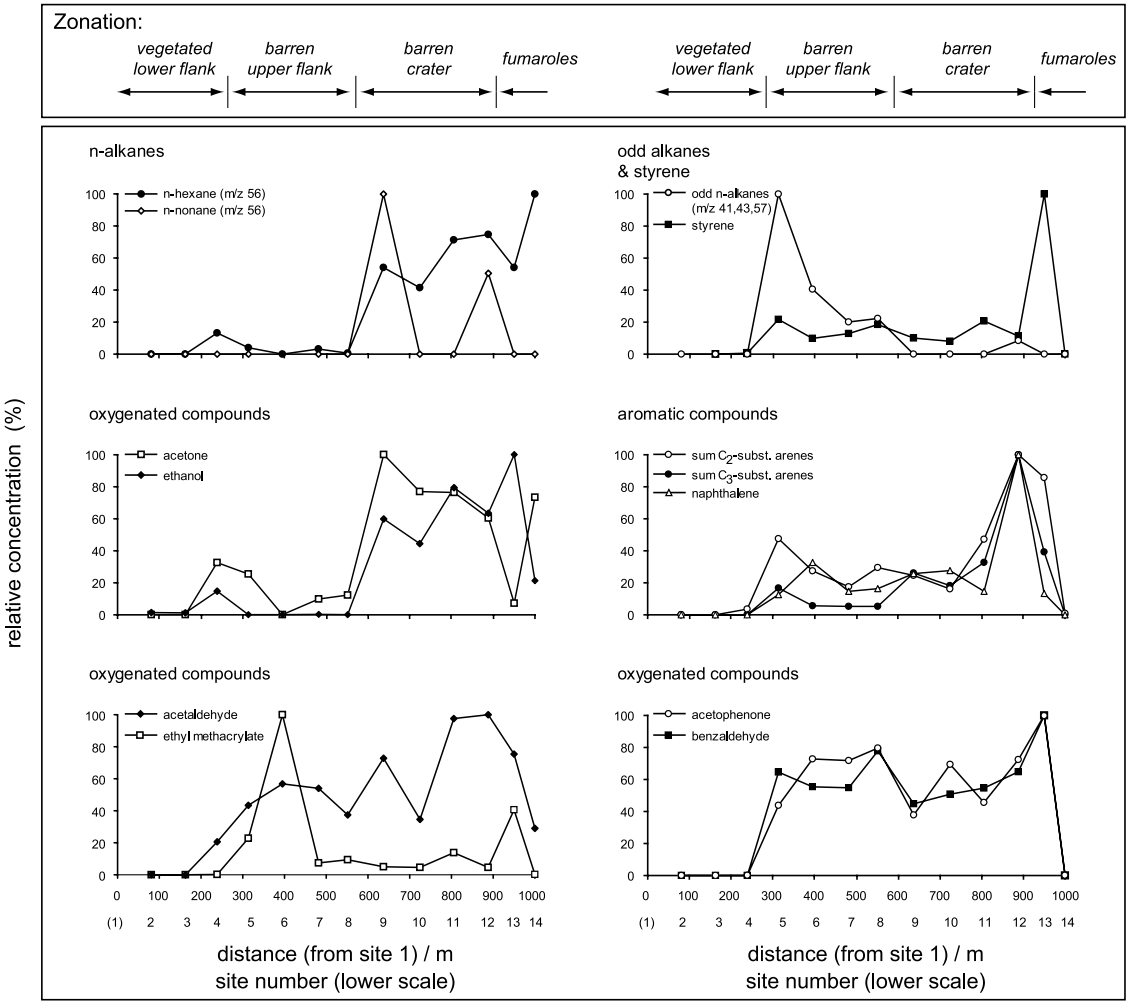

Figure 7. Hydrocarbons and oxygenated compounds present in diffuse emanations (soil gases) on the different sections/zones along the profile. The ordinate in each diagram displays relative concentrations based on integrated peak areas measured with the GC-MS system, in percent of the largest signal obtained. The abscissa refers to the distance from site 1, where the profile was started at the base of the flank of the volcano. The extent of the different zones crossed by the profile are indicated on the top and further explained in the text. Integrated peak areas were corrected for sampled volumes for each site. Instrumental precision was 5% or better.

the calibration curve cancels out in the conversion and the integrated peak area, A_i, is proportional to the mass of the compound on the column, m_i (equation (3)):

$$A_i \propto m_i. \tag{3}$$

[28] If one considers two integrated peak areas, A_1 and A_{max}, that are related to their corresponding compound masses, m_i and m_{max}, on the GC column through a linear calibration curve (equation (4)),

$$m_i = zA_i, \tag{4}$$

their relationship is expressed by the following two terms (equations (5) and (6)),

$$m_i = zA_i \tag{5}$$

$$m_{\max} = zA_{\max} \tag{6}$$

[29] Solving both equations for the slope z, a constant for linear calibration curves results in an unbiased equality of the ratios of maximum and compound masses, to that of the maximum and compound integrated peak areas (equation (7)):

$$\frac{m_i}{m_{\max}} = \frac{A_i}{A_{\max}} \tag{7}$$

Consequently, the following two expressions are equal as well (equation (8)):

$$\frac{m_i}{m_{\max}} \times 100 = \frac{A_i}{A_{\max}} \times 100 \tag{8}$$

[30] Equation (8) (see equation (2)) demonstrates that the values calculated for integrated peak areas of compounds and displayed as percent ''abundances'' of the maximum observed peak area reflect the same relative

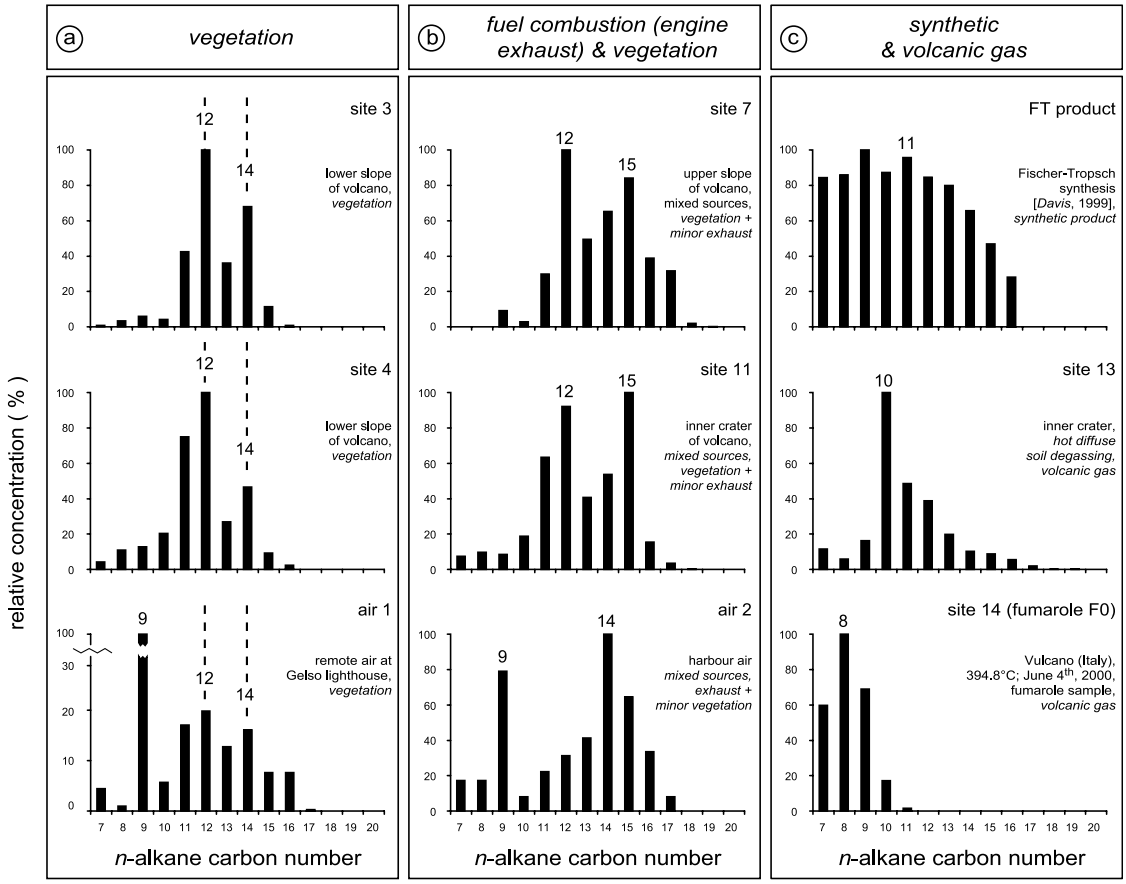

Figure 8. Normal (straight-chain) alkane molecular carbon number distributions for selected representative samples from the profile (i.e., three different sources). The abscissa refers to the number of carbon atoms in the normal alkanes (*n*-alkane) found in each sample (only 1 compound per *n*-alkane carbon number is possible). The ordinates display relative concentrations, based on integrated peak areas relative to the strongest peak in the carbon number range C_7-C_{20}, in percent. The uppermost graph in Figure 8c displays peak heights obtained from published data. Instrumental precision was 5% or better.

trend information through the profile as do the concentrations. Therefore the maximum observed integrated peak area of a compound for a set of samples defines the maximum concentration for the same set of samples (Figures 7–10). This is based on the assumptions that the integrated peak areas are within the linear range of the detector (which is highly likely if distinct integratable peaks are present in the RIC), that the instrumental drift is negligible or corrected for, and that the calibration curve is a linear function. This is usually the case for GC-MS data, has been observed for the compounds quantified such as CFC-11 and is to be expected on the basis of equation (3).

[31] In Figure 8, *n*-alkane carbon number distribution patterns are shown for a representative selection of sites that are characterized by varying influences of volatiles from vegetation, fuel exhaust, and volcanic gas. These diagrams help to distinguish the sources and processes giving rise to the organic chemistry found at the various sites. In Figure 6 and 11 a selection of well correlated compounds and CO_2 flux are displayed. We calculated and ranked a correlation matrix of over 100 compounds and physical parameters in order to gain insight into processes by which physical and chemical signals seem to be related. Only a representative selection can be presented here.

3.2.1. Hydrocarbons

[32] The first row of Figure 7 shows the results for *n*-alkanes and styrene and the remaining diagrams display the results for aromatic hydrocarbons (arenes) and oxygenated compounds along the profile. Normal alkanes (*n*-alkanes) are straight-chain aliphatic saturated hydrocarbons of the general formula C_nH_{2n+2}. The *n*-hexane concentration is markedly increasing toward the crater. The concentrations of *n*-nonane are more variable from one site to the other but generally increase toward the crater as well, with pronounced maxima over sites of active subsurface degassing (crater ring fault at site 9). Hexane is a prominent hydrocarbon found in a variety of low-temperature volcanic and hydrothermal degassing sites around the world [*Capaccioni et al.*, 1993; *Kiyoshu and Asada*, 1995], whereas *n*-nonane dominates other hydrocarbons in air near vegetation (see Figure 8a, air 1). Despite the relative dominance of *n*-nonane over other *n*-alkanes at sites influenced by vegetation, the absolute concentrations nevertheless notably increase toward the crater, indicating that the relatively weak signal from the vegetation is quickly overwhelmed by subsurface degassing.

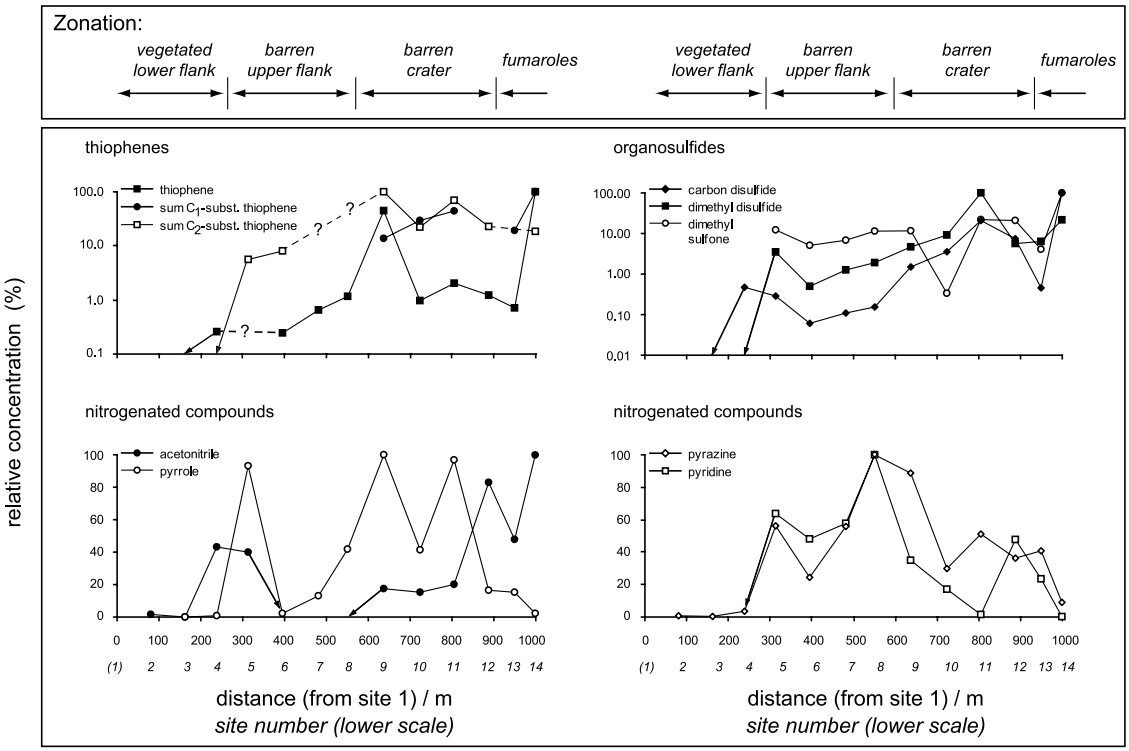

Figure 9. Heteroatomic (S, N) organic compounds present in diffuse emanations (soil gases) on the different sections/zones along the profile. Abscissa and ordinate are as in Figure 7; note that the upper two diagrams have a logarithmic scale on the ordinate. Further details are given in the text and in Figure 7. The dashed lines connect sites between which data points are not given. These "missing" data points (indicated by question marks) are detected compounds that could not be quantified with a reasonable degree of confidence due to overlaps with coeluting peaks with similar mass fragments. Instrumental precision was 5% or better.

Interestingly, *n*-butane (not shown) shows an apparent variation with atmospheric pressure of the sampling site in all samples which is considered to be an artifact.

[33] The even/odd predominance of biological organic matter is a common phenomenon used to assess maturation of fossil fuels derived from terrestrial plants. However, this signature is destroyed/altered by hydrous pyrolysis [*Putschew et al.*, 1998]. Terrestrial plants synthesize complex organic compounds *via* polymerization of acetic acid (among other pathways such as isoprene polymerization), eventually leading (statistically) to a dominance of even carbon-numbered compounds. In addition, no even/odd predominance is observed for abiogenically synthesized compounds (e.g., via Fischer-Tropsch reaction). In the uppermost right diagram in Figure 7 the abundance of odd numbered *n*-alkanes decreases toward the crater, however, it is somewhat lower in the vegetated zone itself. The highest abundances are found on the upper flank of the volcano but they decrease toward the crater bottom.

[34] In Figure 8 a strong even/odd predominance can be seen to be present in the samples from the vegetated zone, even though the total abundance of odd alkanes is not elevated (Figure 7). The strong signal of odd hydrocarbons must therefore have a second source in addition to plant volatiles. In Figure 8, samples from the upper slopes as well as within the crater resemble a mixture of fuel combustion exhaust volatiles (represented by the Vulcano harbor air sample) and plant derived volatiles with a strong C_{12} peak similar to sites 3 and 4 (Figure 8).

[35] Further information on the *n*-alkanes can be extracted from Figure 8, including a high-temperature fumarole at site 14 (394.8°C fumarole F0), and a remote Vulcano air sample (taken at the shore near vegetation at Gelso, on the south coast of the island of Vulcano). A polluted air blank taken in Vulcano harbor during ferry loading and vehicle traffic is also shown. For comparison, a synthetic Fischer-Tropsch product is shown as well [*Davis et al.*, 1999].

[36] The samples from the vegetated zone (sites 3 and 4 in Figure 8a) display a systematic abundance alteration of odd and even hydrocarbons, documented by significantly lower abundances of adjacent carbon numbers to the prominent C_{12} and C_{14} peaks. This pattern appears to indicate a dominance of biogenic organic matter. The hydrocarbon curve has its maximum at about C_{12}, shifting toward heavier molecular weight hydrocarbons at site 6 (not shown). The remote air sample (Gelso air) taken near vegetation also has maxima at C_{12}, C_{14}, and C_9.

[37] Sites 7 through 12 are characterized by a gently rising/falling hydrocarbon distribution, centered at C_{14}, with a two prominent additional peaks at C_{12} and C_{15}. The harbor air sample exhibits a pronounced maximum at C_{14} as well, suggesting an anthropogenic source of a significant portion of the hydrocarbons in soil gases on the upper flanks of the La Fossa cone (sites 7–12). The harbor air with its

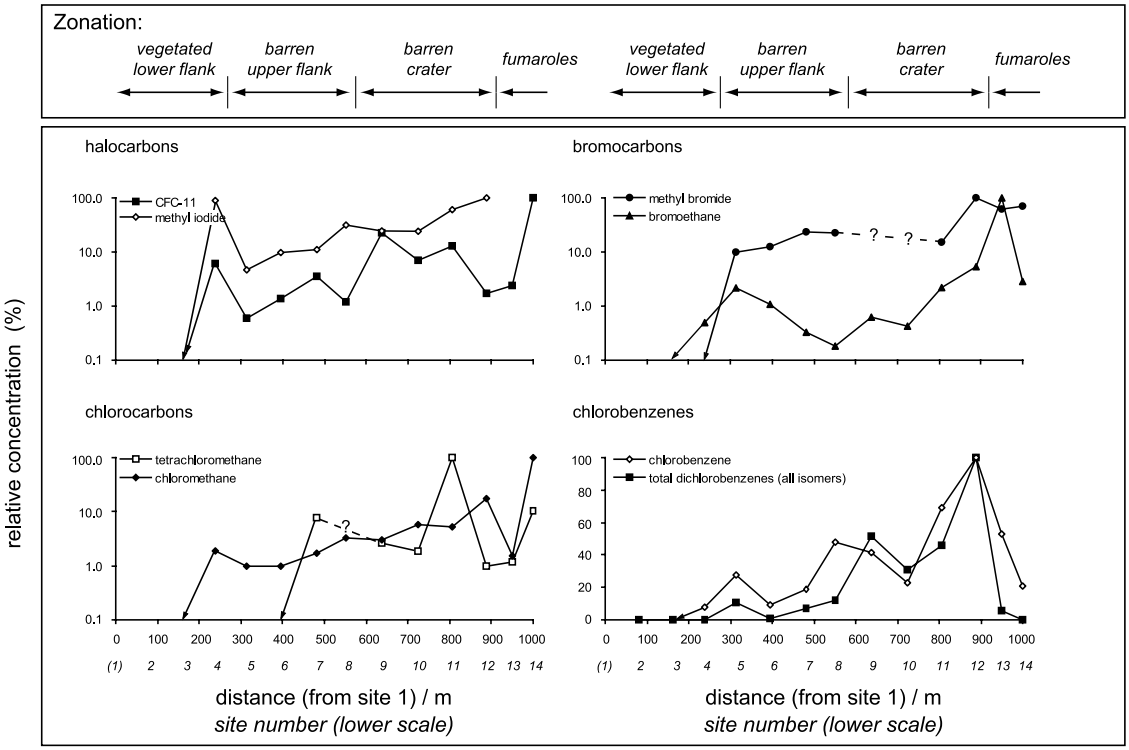

Figure 10. Halocarbon compounds present in diffuse emanations (soil gases) on the different sections/zones along the profile. Abscissa and ordinate are as in Figure 7; note that the upper two and the lower left diagrams have a logarithmic scale on the ordinate. Further details are given in the text and in Figures 7 and 9. Instrumental precision was 5% or better.

relatively heavy *n*-alkane distribution is dominated by the products of incomplete combustion of diesel fuel from the commercial vehicle traffic and the ferry engines.

[38] The fumarolic gas sample (site 14, fumarole F0) is very reducing in nature with excess, detectable, free hydrogen gas. Its hydrocarbon distribution has its modus at C_8, with abundances sharply linearly falling with increasing molecular weight. This type of pattern resembles the Schulz-Flory distribution [*Satterfield and Huff*, 1982] which is regarded as a strong indicator of the abiogenic catalytic Fischer-Tropsch synthesis [*Salvi and Williams-Jones*, 1997]. For comparison, a product of this process is shown in Figure 8c (FT product) displaying the Schulz-Flory distribution and a number of synthetic polymers of lower molecular weight. In the example shown, only CO and H_2 were used to synthesize these compounds over an iron-based catalyst [*Davis et al.*, 1999]. The modus location and slope of the Schulz-Flory distribution depends on the experimental conditions such as temperature, humidity, oxygen fugacity, type of alloy of catalyst, and gas feed composition. In contrast to such Fischer-Tropsch synthesized, linearly falling *n*-alkane patterns, pyrolysis (both confined and hydrous) of biogenic material produces gently exponentially falling *n*-alkane patterns at the temperatures currently typical for the Vulcano fumaroles, ~400°C [e.g., *Schlepp et al.*, 2001]. We therefore consider that this fumarolic gas sample (site 14) may be the result of abiogenic formation of hydrocarbons in the gas phase.

3.2.2. Aromatic Compounds (Arenes)

[39] A number of aromatic compounds, including polycyclic aromatic hydrocarbons (PAH), have been reported from volcanic gases [*Schwandner et al.*, 2001b] but they also may typically derive from anthropogenic or biogenic sources. Benzene, toluene, ethylbenzene, and the xylenes (BTEX), styrene, substituted arenes, naphthalene and higher

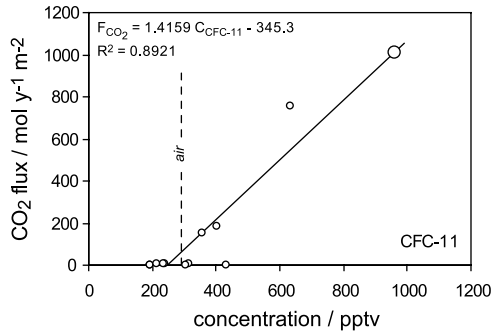

Figure 11. Quantitative correlation diagram of volume-corrected CFC-11 concentrations of all sites along the profile except the fumarolic gas from site 14 (fumarole F0). The ordinate shows the measured CO_2 flux at each site, and the abscissa displays CFC-11 concentrations in adsorbent cartridge samples taken at the same location and time. The hatched line indicates the average tropospheric CFC-11 concentration (see Figure 12). The correlation function and R^2 correlation coefficient were obtained from linear least squares regression of the data. Symbol diameters are larger than analytical uncertainties (about 2.4% for CFC-11, <2% for CO_2 flux), and the symbols are sized accordingly. Instrumental precision was 5% or better.

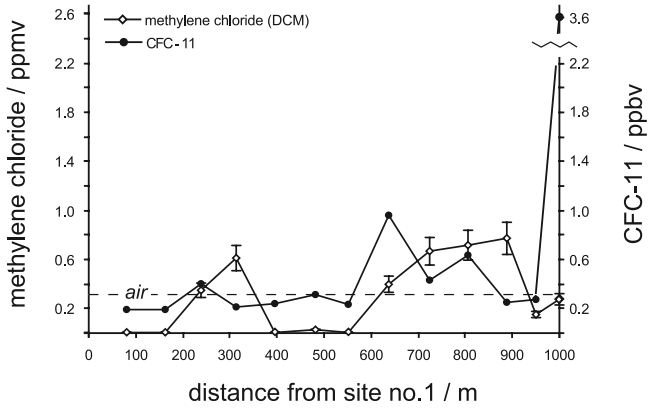

Figure 12. Quantitative variations of halocarbon concentrations (methylene chloride and CFC-11) present in diffuse emanations (soil gases) on the different sections/zones along the profile. The abscissa is the same as in Figure 7, and the two different ordinates refer to concentrations in ppbv (for methylene chloride) and pptv (for CFC-11). The dashed line represents the average tropospheric CFC-11 concentration; however, the soil gas samples and ambient air blanks not included in this diagram indicate that the actual local concentration may be only around 200 pptv. The errors for the CFC-11 data are smaller than the symbol size (see Table 1). Further details are given in the text and in Figure 7. Instrumental precision was 5% or better.

PAHs and their hydrated derivatives are found in our samples. All of these compounds increase in abundance toward the crater (Figure 7), but are relatively low in volcanic gases. Blank readings are very low and diffuse flank degassing appears to be a significant source of these compounds. In contrast to this pattern, styrene is consistently found at low concentration throughout the profile with a pronounced single peak at site 13 (a site of diffuse but >80°C degassing).

3.2.3. Oxygenated and Nitrogenated Compounds

[40] Among the oxygenated compounds (Figure 7), ketones and alcohols show a strong enrichment toward the crater area. Acetophenone (C_8H_8O) is, in addition, enriched on the upper flanks of the cone. All trends of oxygenated compounds except ethyl methacrylate show a clear enrichment toward the crater. Acetone correlates reasonably well with the measured CO_2 flux, indicating a volcanic origin (Figure 6). Ethyl methacrylate ($C_6H_{10}O_2$) does not show any similarity to any other physical or chemical signal and is generally of uniformly low relative abundance (Figure 7). It is a common contaminant derived from adhesives and plastics, such as present in the SPME fiber and the analytical column. It most probably is a procedural contaminant. Acrolein (2-propenal) appears to correlate with ethanol (Figure 6), which is strongly biased toward the crater area (Figure 7). Both compounds may thus have a strong volcanic contribution as well. Acetaldehyde (ethanal) shows a recognizable correlation with dimethyl sulfone (Figure 6), some of the scatter possibly being attributable to oxidation of dimethyl sulfide to yield excess dimethyl sulfone (section 3.2.4).

[41] The second row of Figure 9 demonstrates that the nitrogen containing heterocycles pyridine (C_5H_5N), pyrazine ($C_4H_5N_2$) and pyrrole (C_4H_5N) are enriched on the upper flanks of the volcano but decrease from the crater rim toward the fumaroles which contain lower concentrations, with a pronounced increase at the crater bottom. Pyridine and pyrazine exhibit this pattern more strongly than pyrrole. Acetonitrile (C_2H_3N) is plotted as a representative of several nitriles found in the samples and is enriched in the volcanic gases. Acetonitrile and methyl bromide appear to correlate reasonably well (Figure 6), however, too few samples contained enough methyl bromide to produce a statistically relevant regression for this correlation.

3.2.4. Sulfur Compounds

[42] Volcanic gases contain sulfur as a major element in various forms and native sulfur and sulfide phases typically sublime around fumaroles. Sulfur in volcanic gases occurs predominantly as SO_2, COS, and H_2S. However, we have also identified organosulfur compounds. Row 1 of Figure 9 shows a notable increase of all organosulfur compounds toward the crater with a strong enrichment in the volcanic gases. The organosulfides additionally show an enrichment above inferred or known faults and in areas of fumarolic activity.

[43] The oxygenated compound dimethyl sulfone ($C_2H_6O_2S$) was also identified on the upper flanks of the cone but was diminished in the vegetated area at the base of the profile. Dimethyl sulfide (C_2H_6S) was found in several fumarolic gas samples [*Schwandner et al.*, 2001b] but not detected along the profile. Trace dimethyl sulfide was also detected in the site 1 gas sample which was analyzed at higher resolution. The dimethyl sulfide concentrations are probably slightly higher in the volcanic gas inside the volcanic edifice since dimethyl sulfide is readily oxidized to dimethyl sulfone once it enters the atmosphere.

[44] All sulfides (as well as some arenes and halocarbons) show a small peak at site 4 at the onset of visible vegetation on the slope (note: Logarithmic scale). Apparent resistivities are elevated at this site as well (Figure 5), indicating a local subsurface gas-rich feature such as an active fault buried by slope debris. The heterocyclic thiophenes were not detected in samples from the vegetated lower flanks of the cone but are relatively prominent in the volcanic gases and on the upper volcanic flanks. Thiophene (C_4H_4S) and its C_2- and C_3-substituted derivatives were not only found enriched in the crater area and the volcanic gases, but they also correlate well with the CO_2 flux, indicating a volcanic origin (Figure 6).

3.2.5. Halocarbons

[45] The halocarbons (Figure 10) increase in abundance from the flank toward the crater, with in some cases dramatic increases in the volcanic gas samples (note the logarithmic scale of some of the diagrams in Figure 10). All three methyl halides, CH_3Br, CH_3I and CH_3Cl, show enrichment toward the fumaroles and CH_3I is already notably enriched in crater soil gases (Figure 10). CH_3I and CH_3Cl abundances correlate well (Figure 6c), supporting a volcanic origin consistent with the apparent strong enrichment in the fumarolic area. Bromoethane, C_2H_5Br, is most prominent at site 13, in an area where strong diffuse gas emanation (hissing sound) was observed with temperatures in the range from 80 to 100°C near the surface sampling site. This suggests a possible lower temperature of formation for bromoethane in this environment than for methyl

bromide which is more pronounced at the much higher temperatures of the fumarolic volcanic gases.

[46] Increased methylene chloride, CH_2Cl_2, concentrations are associated/correlated with elevated ground resistivities (see Figures 5 and 12), indicating a subsurface origin. Methylene chloride reaches diffuse gas concentrations as high as 800 ppbv but is not any more enriched in the volcanic gas of site 14. CFC-11 (CCl_3F) also correlates well with CO_2 degassing (Figure 11), but in contrast to methylene chloride is also present at high concentrations in the volcanic gases (Figure 12). At the bottom of Figure 10, data for chlorinated benzenes (monochlorobenzenes and dichlorobenzenes) are shown. The sum of all three dichlorobenzene ($C_6H_4Cl_2$) isomers as well as chlorobenzene (C_6H_5Cl) show a clear increase toward the crater but a smaller abundance in the volcanic gases. The chlorobenzenes appear to have a much stronger source in diffuse rather than fumarolic degassing.

[47] Tetrachloromethane, CCl_4, (Figure 10, lower left) was not detected at the vegetated base of the profile but was detected in the crater area and in fumarolic discharges. Pronounced peaks are evident at site 11 (inner crater rim) and in the fumarolic gas (site 14, fumarole F0), strongly indicating a subsurface source. The other crater sites (i.e., sites 9, 10, 12, 13) are all at similar concentration, indicating a deep rather than shallow formation of this compound. The same applies to site 7, where despite the very impermeable "Fossa Rossa" volcanic ash substrate, small scale sublimation phenomena can be observed along cracks.

[48] Figure 12 shows quantitative data of concentration variations along the profile for methylene chloride and CFC-11. Methylene chloride, CH_2Cl_2, shows a strong enrichment toward the crater, but no pronounced enrichment in fumarolic gas, whereas CFC-11 is enriched by an order of magnitude over background air and even over average crater soil gas concentrations in the fumarolic discharges. The dashed line represents the average tropospheric CFC-11 concentration, however, the soil gas samples and ambient air blanks (not included in this diagram) indicate that the actual local concentration may be only around 200 pptv.

[49] In both cases (average tropospheric air or local air with 200 pptv), the volcanic gas as well as a number of samples of soil gases from the crater area are significantly enriched in CFC-11 and cannot be derived from air contamination. The air component for the fumarolic gas considered in this study was found to be less than 0.001% based on He and Ne isotopic analyses and He, Ne, Ar and N_2 atomic ratios of headspace analyses of volcanic gases sampled by conventional methods ("Giggenbach bottle") from the same sampling train.

[50] Figure 11 shows a positive correlation of CFC-11 concentration to CO_2 fluxes measured at the sampling site (R^2 = 0.89, slope = 1.42 ± 0.1). The strength of the correlation is mainly controlled by four data points and a data point group: The three elevated values at sites 9, 11, and 4, and the data point group near the intercept, close to air concentrations. Site 10 was not included in this correlation because it constitutes a significantly odd value in the diagram and some minor problems were encountered during sampling: The underground sealing of the probe was not sufficient and a layer of lose gravel increased the pore space volume. Concentrations and integrated peak areas of this site are probably an underestimate for trace gases, but correct for the CO_2 flux. The low uncertainty of the correlation function slope demonstrates its unambiguous significant deviation from unity. This deviation is due to the values of low to zero CO_2 fluxes having corresponding CFC-11 values around 200–400 pptv. This observed phenomenon is most likely due to the CFC-11 concentration in the stagnant shallow soil gas being greater than zero, near the ambient air concentration (dashed line). The correlation curve intercepts the CFC-11 concentration axis in the same area, at ~250 pptv, within the range of measured soil gas concentrations with extremely low or zero CO_2 fluxes. This consistency indicates that the shallow soil gas is probably in osmotic equilibrium with ambient air. In contrast, higher CO_2 fluxes correspond to significant increases in CFC-11 concentrations. This observation as well as the above mentioned strong enrichments in the crater area, especially in the fumarolic gases, documents a deep, abiogenic and nonatmospheric origin of this compound. In addition, this correlation allows quantification of fluxes for individual volcanoes and on a global scale (F. Schwandner et al., manuscript in preparation, 2004).

3.2.6. Botanical Observations

[51] In order to assess the influence of the vegetation on the volatile organic chemistry of the samples, we carried out a plant collection in autumn 2001. We found the visible vegetation not only to be limited to the first four sampling sites, but also strongly zoned despite the apparently similar substrate conditions (soil material, slope, etc.). At the base of the profile, a great variety of grasses and few thistles dominate but are quickly replaced by *Leguminosae*, dominated by woody *Genista* sp. brooms (including *Spartium junceum*) as one moves upslope. Since *Leguminosae* are not nitrogen-limited and appear to dwell under elevated CO_2 atmospheres [*Lüscher and Nösberger*, 1997; *Gloser et al.*, 2000]; an actual local advantage can be postulated. Thus vegetation zonation on volcanic slopes may indicate subsurface degassing structures. In the organic trace chemistry of the soil gases, several terpenes and terpenoids were identified, some of which are characteristic for *Leguminosae*. Among the terpenes found in sites 1–4 soil gases are alpha-copaene and ylangene (isomers, tricyclic sesquiterpenes), camphene, limonene, pinene, alpha-terpinene, isolongifolene, alpha-gurjunene, alpha-phellandrene, beta-myrcene, tricyclene, and several others. However, some were also found in minor quantities at the upper slopes of the profile, perhaps having been adsorbed onto the volcanic ash particles. Some typical "plant volatile" compounds, such as cumene (isopropylbenzene), found on the upper slopes may also be of either pristine volcanic or anthropogenic origin.

4. Summary and Discussion

[52] The physical and chemical data presented in this study show that distal airborne fumarolic volcanic gases and on-site vegetation are not the only contributors to organic trace gases found in soil gas. A subsurface source associated with diffuse degassing structures appears to be a newly discovered source, based on data presented in this study. The investigated soil gas profile can be subdivided into four

major zones: The vegetated base of the profile with a granular loose lapilli and ash substrate, the unvegetated upper flanks of the volcanic cone with different substrates of volcanic material, the vegetation-free crater area with cemented pyroclastic and loose epiclastic substrates and strong diffuse degassing features, and fumarolic areas including discrete volcanic gas emanations from fumaroles.

4.1. Vegetation Effects and Adsorption on Soil Particles

[53] Vegetation-derived volatile organic trace gases dominate the soil gas chemistry of the vegetated base of the volcanic cone of La Fossa. Among them are terpenes and terpenoids, nitrogenated compounds and C_9-dominated hydrocarbons, with an apparent even/odd predominance, as well as dimethyl sulfide and carbon disulfide. The organic content of soil gases from the upper flanks of the volcanic ash slopes are dominated by what appears to be adsorbed organic matter derived from a variety of remote and local sources, including anthropogenic atmospheric background contaminants, airborne proximal plant organic volatiles from the base of the cone, anthropogenic emissions from fuel combustion, and a component attributable to volcanic emanations.

[54] The vegetation-derived compounds on the upper flank consist of *n*-alkanes, aldehydes, ketones (except acetone), nitrogenated heterocycles, terpenes, and dimethyl sulfone as an oxidation product of dimethyl sulfide. The anthropogenic component is best characterized by the *n*-alkane distribution in the harbor air sample (Figure 8, "air 2"). This sample represents a mixture of vegetation-derived volatiles (i.e., strong C_9) and an alkane normal distribution with a maximum at C_{14}. Traces of its *n*-alkane distribution are partially recognizable at sites 7 and 11 as well (Figure 8), mixed with a small vegetation-derived component indicated by a C_{12} peak. The volcanic gas component consists of arenes, acetone, halocarbons, ethanol, and thiophenes. No overprint of volcanogenic *n*-alkane distributions (site 14) can be identified on the upper slopes.

[55] The airborne "atmospheric" component responsible for compounds found on the upper slopes and to much lesser extent in the crater, manifests itself in compounds that are probably adsorbed onto soil particles. The sources of this airborne component are all of the above-mentioned individual sources, including volcanic gas. If one theoretically considers that the volcano would be temporarily "switched off", concentrations of some compounds would probably be decreasing toward the crater after equilibration with the local atmosphere. The background signal of halocarbons derived from the atmosphere (and thus by large anthropogenic sources) would encounter a soil substrate that has a drastically reduced surface availability for adsorption due to its previously cemented character. In our study, we see no evidence for atmospheric halocarbons at significant concentrations relative to the other local strong sources. In contrast, we observe that the halocarbons derived from subsurface degassing dominate the organic chemistry of the volcanic soil gases.

[56] For example, the tetrachloromethane (CCl_4) concentrations would be expected to be of the same concentration throughout the entire profile if one attempted to explain the observed CCl_4 concentrations by a nonvolcanic, remote atmospheric, source. This is obviously not the case since strong peaks are observed at sites of known structures of subsurface degassing (in this study confirmed by CO_2 flux and resistivity data) and the base of the profile is free of detectable CCl_4. In addition to the uniform concentration profile expected of the remote atmospheric interpretation, CCl_4 concentrations should actually be elevated at sites dominated by vegetation (sites 1–4), because tetrachloromethane retention in soils is strongly controlled by its organic carbon content [*Duffy et al.*, 1997] and the substrate of sites 5–14 is extremely poor in organic carbon. However, no CCl_4 was detected in the samples from the vegetated zone.

[57] Any supposed adsorbed halocarbons on soil particles are clearly overwhelmed by a strong volcanic signal, even though the dry climate of the Aeolian Islands actually facilitates enrichment of halocarbons in the shallow soil. It was found experimentally that by adsorbing volatile organic compounds, the total volatile organic carbon sorption capacity of soil minerals at low water content increases by several orders of magnitude, for some compounds including trichloroethylene [*Poulsen et al.*, 2000]. The dry climate of the Aeolian Islands during the summer requires a separate control on adsorption in organic carbon-poor volcanic ash. One such facilitating process could be intraparticle mass transfer which affects the adsorption process at sites with mostly coarse-grained substrate character, such as the upper flank regions [*Chen and Wu*, 1995]. The only remaining possible explanation other than subsurface degassing would be a local anthropogenic source of CCl_4 but this hypothesis is not verified by the harbor air sample and the reasoning presented above.

[58] Nitrogenated compounds show enrichment patterns favoring the upper flanks (for heterocyclic compounds) or the crater and fumaroles (for nitriles). In this case, the local volcanic source is by far dominant. The presence of acetonitrile in soils facilitates pyridine adsorption on soil particles [*Borisover et al.*, 2001], but this coupled effect does not explain the observed enrichment patterns since acetonitrile increases toward the crater and pyridine in contrast decreases toward the crater. A local strong volcanic source of acetonitrile would therefore be the only explanation for the observed enrichment of this nitrile.

4.2. Crater Region

[59] The crater region is characterized by a high diffuse gas flow. Individual sites of elevated gas discharge (at either site 9 or the fumarole, F0, at site 14) produce peaks that are strongest for CFC-11, *n*-hexane, CCl_4, thiophene, CH_3Cl, CS_2, and the chlorobenzenes. Hexane increasingly dominates the *n*-alkanes discharge with proximity to fumaroles. Strong bimodal patterns in the *n*-alkane distribution are not noted. The vegetation indicator *n*-nonane (C_9) dominates the soil gas alkane chemistry at the vegetated sites at the base of the profile and loses this dominance relative to other alkanes in the crater area. The absolute *n*-nonane concentration, however, increases toward the crater as well, indicating a strong volcanic source. The *n*-alkane distribution is dominated by C_{12}-C_{15}.

[60] All halocarbons show elevated values in the crater. The increase is less pronounced for CCl_4 (see above) and methyl chloride but quite strong for methyl iodide and -bromide, methylene chloride, CFC-11 and the chloro-

benzenes. Strong general increases and strongly elevated concentrations are observed for halocarbons, acetone, acetonitrile, acetaldehyde and ethanol among others. All the halocarbons except the haloarenes and bromoethane show their strongest enrichment in the volcanic gas-dominated emanations (fumarole fields and fumaroles). The same applies to thiophene and its substituted derivatives, dimethyl disulfide and acetonitrile. In areas of active fumarolic degassing, styrene, C_2-substituted arenes, acetophenone, benzaldehyde, methyl bromide and bromoethane are strongly enriched where intense, diffuse warm ($\sim$80–100°C) degassing occurs (i.e., site 13). The very reducing volcanic gas sampled at fumarole F0 (site 14) bears no resemblance to any of the nonvolcanic sources, and its halocarbon concentrations are for chloromethane, CFC-11, and to some extend tetrachloromethane, the highest found in all samples. The *n*-alkane distribution is centered at a lower molecular weight with linearly decreasing abundances with increasing carbon number (Schulz-Flory distribution), suggesting inorganic catalytic Fischer-Tropsch synthesis.

4.3. Abiogenic Formation

[61] Some of the organic compounds with the degree of complexity of those found in volcanic gases may not be stable (i.e., in equilibrium) at the discharge temperatures of the gases themselves but may instead form during cooling of the volcanic gas down to its surface exit temperatures. Other compounds may form later during dilution with air after emission to the atmosphere [*Zolotov and Shock*, 2000]. The thermal stability of many of the relevant organic compounds is poorly known at temperatures >400°C. In our case, the gas is essentially quenched during sampling so that the compounds trapped on the adsorbent cartridge probably represent an equilibrium mixture of higher-temperature conditions [*Symonds et al.*, 1994]. The compounds most likely form from simple organic precursors by gas-phase radical reactions that may be mediated by the available natural catalytic surfaces. Organic precursor molecules may form via catalytic Fischer-Tropsch reaction [e.g., *Brodie*, 1873; *Fischer*, 1935], as indicated by the number of isomers found (F. Schwandner et al., manuscript in preparation, 2004) as well as by the apparent Schulz-Flory distribution in reducing volcanic gas samples as demonstrated by fumarole F0 (site 14). Subsequent gas-phase or catalytic surface aided polymerization may form higher molecular weight compounds condensing on surfaces or being emitted to the atmosphere. Gas phase electrophillic substitution and alkyl free radical reactions may form and modify halocarbons, heterocycles and arenes in the hot volcanic gas.

[62] Many of the arguments presented in this study are supported by strong positive correlations of compound concentration with CO_2 flux. The subsurface degassing operates quasi-continuously on a century to millennia timescale giving rise to very high daily CO_2 discharges at Vulcano (180–230 t d^{-1} [*Chiodini et al.*, 1996]). From the data presented in this study, we conclude that in terms of a volcanic source of halocarbons in the atmosphere, diffuse volcanic emission probably plays a role about equal to that of discrete fumarolic emissions. To estimate the volcanic source strength of halocarbons, the organic composition may be scaled to SO_2 fluxes determined independently by COSPEC-measurements. However, there are shortcomings associated with SO_2 fluxes determined by that method (scattering effects with volcanic sulphate aerosol and sulphate-covered ash particles). Sulphur speciation can be quite variable in a volcanic gas, making it difficult to correlate SO_2 fluxes and SO_2 abundances in the pure fumarolic gas, in that H_2S may in some cases dominate over SO_2. In other cases, the reverse can be observed. CO_2 concentrations in a fumarolic gas are not as variable and even though volcanic C-O-H fluids speciate into CO and CH_4 as well, depending on temperature and redox potential, CO_2 is in most cases the dominating species. In addition, CO_2 fluxes determined indirectly by COSPEC measurement of SO_2 and SO_2/CO_2 COSPEC and gas sample ratio correlation have the advantage of being much more accurate than quantitative COSPEC-SO_2 measurements. Confirmatory CO_2 flux data are available for an increasing number of volcanoes by grid mapping of diffuse soil degassing [e.g., *Koepenick*, 1995; *Chiodini et al.*, 1996, 1998, 2001; *Giammanco et al.*, 1998; *Wardell et al.*, 1999; *Brombach et al.*, 2001].

4.4. Volcanic Halocarbon Source Strength

[63] We previously estimated a global volcanic CFC-11 source strength from quasi-continuous, discrete fumarolic degassing to have a global annual mass flux from volcanoes to the atmosphere of $0.3–1.25 \times 10^{-5}$ Tg y^{-1} (data from *Schwandner et al.* [2001b]). If diffuse degassing contributes approximately the same amount as appears to be the case at Vulcano, the volcanic source strength will double. Some brominated halocarbons are apparently emitted preferentially from hot but strongly diffuse emissions. In the case of methyl iodide, the diffuse emissions might actually supercede the discrete fumarolic discharges, provided the case of Vulcano can be extrapolated to other volcanoes.

[64] We report on improved volcanic halocarbon source strengths, in particular on the previously not known source of diffuse degassing structures in volcanic regions of high heat and CO_2 flux. Source strength (flux) estimates are listed in Table 2. All previous methods by *Symonds et al.* [1988], *Isidorov* [1990], and *Jordan et al.* [2000] used volcanic SO_2 fluxes to scale trace halocarbon concentrations to. All these studies suffered from either significant instrument or air contamination, or were subjected to adverse matrix effects. Strong over- and underestimates are thus likely in their flux values. Our global fumarolic flux estimates in this study, nevertheless take these studies into account, as well as data from our own work (F. Schwandner et al., manuscript in preparation, 2004). With the identification of diffuse degassing as a new, nonfumarolic and nonexplosive volcanic halocarbon source, source strength estimates require a correction to higher values than if only fumarolic emissions were considered. From the qualitative and quantitative results of this study and methods based on balancing known global sinks, sources and budgets for volcanic degassing as outlined by F. Schwandner et al. (manuscript in preparation, 2004), we estimate the global total quiescent (fumarolic and diffuse) volcanic halocarbon source strengths to be $8.56 \pm 4.7 \times 10^{-6}$ Tg y^{-1}, $0.98 \pm 0.47 \times 10^{-6}$ Tg y^{-1}, and $3.41 \pm 1.0 \times 10^{-6}$ Tg y^{-1}, for CFC-11, CH_3Br, and CCl_4, respectively. Other source strength estimates are listed in Table 2. We base our

Table 2. Global Volcanic Halocarbon and Aromatic Source Strengths

			Estimated Global Volcanic Source Strength						
Compound	Formula	Figure	This Study Fumarolic,[a] Mg y^{-1}	This Study DDF[b]	This Study Diffuse, Mg y^{-1}	J00,[c] Mg y^{-1}	W97,[c] Mg y^{-1}	I90,[c] Mg y^{-1}	S88,[c] Mg y^{-1}
Methyl iodide	CH_3I	6c, 10	1.248 ± 0.8	0.1	0.1 ± 0.1				
Methyl bromide	CH_3Br	6d, 10	0.776 ± 0.5	0.2	0.2 ± 0.1				
Methyl chloride	CH_3Cl	6c, 10	73.85 ± 45	0.05	3.7 ± 2.3	12			$<1 \times 10^{-6}$
Methylene chloride	CH_2Cl_2	12	7.0 ± 4.3	2	14.0 ± 8.6		327		$<5 \times 10^{-12}$[e]
Trichloromethane	$CHCl_3$	4	45.2 ± 28	1.1	49.7 ± 30.4		0.55		$<4 \times 10^{-18}$[e]
Tetrachloromethane	CCl_4	10	1.707 ± 1.0	1	1.7 ± 1.0		17		$<5 \times 10^{-25}$[e]
Trichlorofluoromethane	CCl_3F	10, 11, 12	7.76 ± 4.7	0.1	0.8 ± 0.5	<0.3	306	94[d]	$<2 \times 10^{-24}$[e]
Bromoethane	C_2H_5Br	10	n.q.[f]	0.7	n.q.[f]				
Chlorobenzene	C_6H_5Cl	10	4.24 ± 2.6	2	8.5 ± 5.2				
p-dichlorobenzene	$C_6H_4Cl_2$	10	0.237 ± 0.1	30	7.1 ± 3.0				

[a]Fumarolic source strength, based on average global analyte concentrations in fumarolic emissions (F. Schwandner et al., manuscript in preparation, 2004).

[b]Diffuse degassing factor, relating the average integrated diffuse analyte concentration to that in fumarolic gases: This value is used to calculate the diffuse source strengths based on the fumarolic source strengths and the observation that diffuse and hydrothermal CO_2 release amounts to comparable emissions as in fumarolic degassing [*Kerrick et al.*, 1995].

[c]Data from the literature: J00, *Jordan et al.* [2000]; W97, *Wahrenberger* [1997]; S88, *Symonds et al.* [1988]; I90, *Isidorov* [1990].

[d]This value was recalculated from an estimated burden of 17 pptv for preindustrial volcanogenic CFC-11 in the atmosphere by *Isidorov* [1990], who based his estimate on work by *Khalil and Rasmussen* [1982].

[e]These values were calculated based on fugacity data, assumptions, and methods described by *Symonds et al.* [1988].

[f]Here n.q. is not quantified.

estimates on the global volcanic source strength of CO_2 to be 66 to 78 Tg y^{-1} [*Stoiber*, 1995] and on the assumptions that the CO_2-halocarbon correlation can be globally extrapolated, and that the slope of this correlation is constant. CO_2 flux correlations to CH_3Br and other compounds follow the same procedure and assumptions. Diffuse CO_2 fluxes in regions of high-heat flow are globally similar to subaerial fumarolic degassing [*Kerrick et al.*, 1995], and diffuse fluxes are therefore approximated the same way.

[65] In order to contribute to the natural atmospheric Br budget in a comparable natural source strength as the oceans, the average volcanic gas would have to at least contain 2 ppmv CH_3Br under the same conditions and an average global annual gaseous volcanic CO_2 release of 66 Tg y^{-1} [*Stoiber*, 1995; *Schwandner et al.*, 2002]. Our global flux estimate of $0.98 \pm 0.47 \times 10^{-6}$ Tg y^{-1} for methyl bromide is far below that and will probably not account for budgetary imbalances currently under discussion for the global atmospheric methyl bromide budget. However, CH_3Br is not the only volatile gaseous bromine species in volcanic gases, other than HBr which washes out extremely quickly. Recently, *Bobrowski et al.* [2003] have demonstrated that volcanic eruption plumes can emit $BrO^{\bullet}$ radicals (at 1 ppbv gas concentrations) on the order of 73.2 ± 66.8 Mg y^{-1} of molecular bromine. In this study we found several other organic bromine species in fumarolic and quiescent diffuse flank emissions significantly over ambient air concentrations, namely C_2H_5Br and several other yet unidentified bromocarbons. A portion of these compounds that we trapped at the point of emission on the volcano surface may hydrolyze and photolyze to serve as precursors of the gaseous $BrO^{\bullet}$ detected recently at ~1 ppbv in eruption plumes [*Bobrowski et al.*, 2003]. However, the estimated total quiescent organic bromine concentrations that we find (~10 ppbv) exceed this possible sink by far, so that a large fraction of volcanic bromocarbons would enter the troposphere undisturbed and eventually directly contribute to stratospheric ozone destruction. In order to quantify the volcanic source strength of halocarbons to the atmosphere, diffuse and discrete degassing features will have to be investigated on a more representative number of volcanoes to arrive at a more precise global estimate.

[66] **Acknowledgments.** We thank N. Keller, for help during the sampling campaign and J.S. Cox for laboratory help (both ETH-IMP). Josef Nösberger and Matthias Baltisberger (both ETH) are thanked for identification of some collected plant species and botanical advice. Pierre Gex (Lausanne, CH) kindly shared his original geophysical data along our soil degassing profile. ETH Occupational Health and Security Services (ETH-SU) provided some field safety equipment. Reviews by J.S. Cox and three anonymous reviewers are greatly acknowledged. This project was in part supported by SNF (Swiss National Science Foundation) grants 2000-050494.97/1 and 2000-056892.99/1 to V.J.D and T.M.S, by ETH grant 2-77140-00 to T.M.S., and by a SANW (Swiss Academy of Natural Sciences) grant to F.M.S.

References

Bobrowski, N., G. Hönninger, B. Galle, and U. Platt (2003), Detection of bromine monoxide in a volcanic plume, *Nature*, *423*, 273–276.

Borisover, M., M. Reddy, and E. Graber (2001), Solvation effect on organic compound interactions in soil organic matter, paper presented at EUG XI, Eur. Union on Geosci., Strasbourg, France.

Brodie, B. C. (1873), Note on the synthesis of marsh-gas and formic acid, and on the electric decomposition of carbonic oxide, *Proc. R. Soc. London*, *21*(7), 245–247.

Brombach, T. (2000), Fluid geochemistry of hydrothermal systems in volcanic island arcs: Guadaloupe (Lesser Antilles) and Nisyros (Greece), Ph.D. thesis, 114 pp., Univ. de Lausanne, Lausanne, Switzerland.

Brombach, T., J. C. Hunziker, G. Chiodini, C. Cardellini, and L. Marini (2001), Soil diffuse degassing and thermal energy fluxes from the southern Lakki plain, Nisyros (Greece), *Geophys. Res. Lett.*, *28*(1), 69–72.

Bunsen, R. W. (1847), Ueber den inneren Zusammenhang der pseudovulkanischen Erscheinungen Islands, *Ann. Chem. Pharm.*, *62*(1), 1–59.

Bunsen, R. W. (1852), Ueber vulkanische Exhalationen, *Jahrb. Schles. Ges. Vaterl. Kultur*, *30*, 29–30.

Butler, J. H. (2000), Better budgets for methyl halides?, *Nature*, *403*, 260–261.

Butler, J. H., S. A. Montzka, A. D. Clarke, J. M. Lobert, and J. W. Elkins (1998), Growth and distribution of halons in the atmosphere, *J. Geophys. Res.*, *103*(D1), 1503–1511.

Capaccioni, B., M. Martini, F. Mangani, L. Giannini, G. Nappi, and F. Prati (1993), Light hydrocarbons in gas emissions from volcanic areas and geothermal fields, *Geochem. J.*, *27*(1), 7–17.

Chen, C.-Y., and S.-C. Wu (1995), The adsorption of benzene, toluene and ethylbenzene on soils near infinite dilution, *Chemosphere*, *31*(10), 4225–4235.

Chiodini, G., F. Frondini, and B. Raco (1996), Diffuse emission of CO_2 from the Fossa crater, Vulcano Island (Italy), *Bull. Volcanol.*, *58*(1), 41–50.

Chiodini, G., R. Cioni, M. Guidi, B. Raco, and L. Marini (1998), Soil CO_2 flux measurements in volcanic and geothermal areas, *Appl. Geochem.*, *13*(5), 543–552.

Chiodini, G., F. Frondini, C. Cardellini, D. Granieri, L. Marini, and G. Ventura (2001), CO_2 degassing and energy release at Solfatara volcano, Campi Flegrei, Italy, *J. Geophys. Res.*, *106*(B8), 16,213–16,221.

Couch, M. W., C. J. Schmidt, and S. C. Wasdo (2000), A comparison of sampling techniques for VOCs in soil, *Adv. Environ. Res.*, *4*(1), 97–102.

Cruikshank, D. P., D. Morrison, and K. Lennon (1973), Volcanic gases: Hydrogen burning at Kilauea volcano, Hawaii, *Science*, *182*, 277–279.

Davis, B. H., E. Iglesia, A. Li, M. Tu, S. Li, and W. Li (1999), Technology development for iron and cobalt Fischer-Tropsch catalysts, quarterly report (January 1, 1999 to March 31, 1999), pp. 25–71, Univ. of Calif., Berkeley.

Duffy, C. C., D. L. McCallister, and R. R. Renken (1997), Carbon tetrachloride retention by modern and buried soil horizons, *J. Environ. Qual.*, *26*(4), 1123–1127.

Farman, J. C., B. G. Gardiner, and J. D. Shanklin (1985), Large losses of ozone in Antarctica reveal seasonal ClO_x/NO_x interaction, *Nature*, *315*, 207–210.

Fischer, F. (1935), Die Synthese der Treibstoffe (Kogasin) und Schmieröle aus Kohlendioxyd und Wasserstoff bei gewöhnlichem Druck, *Brennst. Chem..*, *16*, 1–11.

Fulignati, P., A. Gioncada, and A. Sbrana (1998), Geologic model of the magmatic-hydrothermal system of Vulcano (Aeolian Islands, Italy), *Mineral. Petrol.*, *62*, 195–222.

Gaffney, J. S. (1995), Volcanic CFCs, *Environ. Sci. Technol.*, *29*(1), A8.

Gerlach, T. M. (1980), Evaluation of volcanic gas analyses from Kilauea volcano, *J. Volcanol. Geotherm. Res.*, *7*, 295–317.

Gex, P. (1992), Etude géophysique des environs du cratère de Vulcano, Italie, *Bull. Soc. Vaudoise Sci. Nat.*, *82*(2), 157–172.

Giammanco, S., S. Inguaggiato, and M. Valenza (1998), Soil and fumarole gases of Mount Etna: Geochemistry and relations with volcanic activity, *J. Volcanol. Geotherm. Res.*, *81*, 297–310.

Giggenbach, W. F., et al. (2001), Evaluation of results from the fourth and fifth IAVCEI field workshops on volcanic gases, Vulcano island, Italy and Java, Indonesia, *J. Volcanol. Geotherm. Res*, *108*, 157–172.

Gloser, V., M. Jezikova, A. Lüscher, M. Frehner, H. Blum, J. Nösberger, and U. A. Hartwig (2000), Soil mineral nitrogen availability was unaffected by elevated atmospheric pCO_2 in a four years old field experiment (Swiss FACE), *Plant Soil*, *227*, 291–299.

Gribble, G. W. (1994), The natural production of chlorinated compounds, *Environ. Sci. Technol*, *28*(7), A310–A319.

Gribble, G. W. (1996), Naturally occurring organohalogen compounds—A comprehensive survey, *Prog. Org. Nat. Prod.*, *68*, 1–423.

Gribble, G. W. (1999), The diversity of naturally occurring organobromine compounds, *Chem. Soc. Rev.*, *28*(5), 335–346.

Gribble, G. W. (2000), The natural production of organobromine compounds, *Environ. Sci. Pollut. Res.*, *7*(1), 37–49.

Harnisch, J., M. Frische, R. Borchers, A. Eisenhauer, and A. Jordan (2000), Natural fluorinated organics in fluorite and rocks, *Geophys. Res. Lett.*, *27*(13), 1883–1886.

Harris, A. J. L., S. B. Sherman, and R. Wright (2000), Discovery of self-combusting volcanic sulfur flows, *Geology*, *28*(5), 415–418.

Isidorov, V. A. (1990), *Organic Chemistry of the Earth's Atmosphere*, 215 pp., Springer-Verlag, New York.

Isidorov, V. A., I. G. Zenkevich, and B. V. Ioffe (1990), Volatile organic compounds in solfataric gases, *J. Atmos. Chem.*, *10*(3), 329–340.

Jordan, A., J. Harnisch, R. Borchers, F. N. Le Guern, and H. Shinohara (2000), Volcanogenic halocarbons, *Environ. Sci. Technol*, *34*(6), 1122–1124.

Keene, W. C., et al. (1999), Composite global emissions of reactive chlorine from anthropogenic and natural sources: Reactive chlorine emissions inventory, *J. Geophys. Res.*, *104*(D7), 8429–8440.

Keller, J. (1970), Carta geologica dell'Isola di Vulcano (Isole Eolie), Regione Siciliana, Firenze, Italy.

Keller, J. (1980), The island of Vulcano, *Rend. Soc. Ital. Mineral. Petrol.*, *36*(1), 369–414.

Keppler, F., R. Eiden, V. Niedan, J. Pracht, and H. F. Schöler (2000), Halocarbons produced by natural oxidation processes during degradation of organic matter, *Nature*, *403*, 298–301, (Correction, *409*, 382, 2001.)

Kerrick, D. M., M. A. McKibben, T. M. Seward, and K. Caldeira (1995), Convective hydrothermal CO_2 emissions from high heat-flow regions, *Chem. Geol.*, *121*(1–4), 285–293.

Khalil, M. A. K., and R. A. Rasmussen (1982), Secular trends of atmospheric methane (CH_4), *Chemosphere*, *11*(9), 877–883.

Khalil, M. A. K., R. M. Moore, D. B. Harper, J. M. Lobert, D. J. Erickson, V. Koropalov, W. T. Sturges, and W. C. Keene (1999), Natural emissions of chlorine-containing gases: Reactive chlorine emissions inventory, *J. Geophys. Res.*, *104*(D7), 8333–8346.

Kiyoshu, Y., and N. Asada (1995), Light hydrocarbons in volcanic gases from the Japanese island-arc, *Geochem. J.*, *29*(4), 231–242.

Koepenick, K. W. (1995), Volatile emissions from Oldoinyo Lengai volcano, Tanzania, M.Sc. thesis, Pa. State Univ., University Park.

Lobert, J. M., and J. Warnatz (1993), Emissions from the combustion processes in vegetation, in *Fire in the Environment: The Ecological, Atmospheric, and Climate Importance of Vegetation Fires*, edited by P. J. Crutzen and J. G. Goldammer, pp. 15–37, John Wiley, Hoboken, N. J.

Lobert, J. M., W. C. Keene, J. A. Logan, and R. Yevich (1999), Global chlorine emissions from biomass burning: Reactive chlorine emissions inventory, *J. Geophys. Res.*, *104*(D7), 8373–8389.

Lüscher, A., and J. Nösberger (1997), Interspecific and intraspecific variation in the response of grasses and legumes to free air CO_2 enrichment, *Acta Oecol.*, *18*, 269–276.

Mercalli, G., and O. Silvestri (1891), Le eruzioni dell'isola di Vulcano, incominciate il 3 Augusto 1888 e terminate il 22 Marzo 1880, *Ann. Uffic. Cent. Meteorol. Geodin.*, *10*(4), 213 pp.

Molina, M. J., and F. S. Rowland (1974), Stratospheric sink for chlorofluoromethanes: Chlorine atom catalyzed destruction of ozone, *Nature*, *249*, 810–814.

Naughton, J. J. (1973), Volcanic Flame—Source of fuel and relation to volcanic gas-lava equilibrium, *Geochim. Cosmochim. Acta*, *37*(5), 1163–1169.

Poulsen, T. G., T. Yamaguchi, P. Moldrup, L. W. de Jonge, and D. E. Rolston (2000), Predicting volatile organic vapor sorption from soil specific surface area and texture, *J. Environ. Qual.*, *29*(5), 1642–1649.

Putschew, A., C. Schaeffer-Reiss, P. Schaeffer, M. P. Koopmans, J. De Leeuw, M. D. Lewan, J. S. Sinninghe Damsté, and J. R. Maxwell (1998), Release of sulfur- and oxygen-bound components from a sulfur-rich kerogen during simulated maturation by hydrous pyrolysis, *Org. Geochem.*, *29*(8), 1875–1890.

Rasmussen, R. A., L. E. Rasmussen, M. A. K. Khalil, and R. W. Dalluge (1980), Concentration distribution of methyl chloride in the atmosphere, *J. Geophys. Res.*, *85*(C12), 7350–7356.

Reeves, C. E. (2003), Atmospheric budget implications of the temporal and spatial trends in methyl bromide concentration, *J. Geophys. Res.*, *108*(D11), 4343, doi:10.1029/2002JD002943.

Reeves, C. E., and S. A. Penkett (1993), An estimate of the anthropogenic contribution to atmospheric methyl bromide, *Geophys. Res. Lett.*, *20*(15), 1563–1566.

Rhew, R. C., B. R. Miller, and R. F. Weiss (2000), Natural methyl bromide and methyl chloride emissions from coastal salt marshes, *Nature*, *403*, 292–295.

Salvi, S., and A. E. Williams-Jones (1997), Fischer-Tropsch synthesis of hydrocarbons during sub-solidus alteration of the Strange Lake peralkaline granite, Quebec/Labrador, Canada, *Geochim. Cosmochim. Acta*, *61*(1), 83–99.

Satterfield, C. N., and G. A. Huff (1982), Carbon number distribution of Fischer-Tropsch products formed on an iron catalyst in a slurry reactor, *J. Catal.*, *73*, 187–197.

Schlepp, L., M. Elie, P. Landais, and M. A. Romero (2001), Pyrolysis of asphalt in the presence and absence of water, *Fuel Process. Technol.*, *74*, 107–123.

Schwandner, F. M., A. P. Gize, T. M. Seward, K. Hall, and V. J. Dietrich (2000), Natural halocarbon compounds in volcanic gases, *J. Conf. Abstr.*, *5*(2), 898.

Schwandner, F. M., A. P. Gize, K. Hall, T. M. Seward, and V. J. Dietrich (2001a), Short path thermal desorption—SPME-CT-GC/MS: Analysis of trace organic compounds present in hot volcanic gases with high sulfur, water and acid matrix, *Chimia*, *55*(7–8), 590.

Schwandner, F. M., A. P. Gize, T. M. Seward, K. Hall, and V. J. Dietrich (2001b), Organic compounds in volcanic gases, paper presented at EUG XI, Eur. Union on Geosci., Strasbourg, France.

Schwandner, F. M., A. P. Gize, T. M. Seward, P. A. Hall, and V. J. Dietrich (2002), Quiescent diffusive and fumarolic volcanic bromocarbon emissions, *Eos Trans. AGU*, *83*(47), Fall Meet. Suppl., Abstract A72C-0186.

Stoiber, R. E. (1995), Volcanic gases from subaerial volcanoes on Earth, in *A Handbook of Physical Constants*, *Ref. Shelf Ser.*, vol. 1, edited by T. J. Ahrens, pp. 308–319, AGU, Washington, D. C.

Symonds, R. B., W. I. Rose, and M. H. Reed (1988), Contribution of Cl-bearing and F-bearing gases to the atmosphere by volcanoes, *Nature*, *334*, 415–418.

Symonds, R. B., W. I. Rose, G. J. S. Bluth, and T. M. Gerlach (1994), Volcanic gas studies—Methods, results, and applications, in *Volatiles in Magmas*, *Rev. Mineral. Geochem.*, 30, 1–66.

Tedesco, D., G. Miele, Y. Sano, and J. P. Toutain (1995), Helium isotopic ratio in Vulcano Island fumaroles: Temporal variations in shallow level mixing and deep magmatic supply, *J. Volcanol. Geotherm. Res.*, *64*, 117–128.

Wahrenberger, C. (1997), Some aspects of the chemistry of volcanic gases, Ph.D. thesis, 233 pp., ETH Zürich, Zurich, Switzerland.

Wahrenberger, C., V. Dietrich, T. M. Seward, I. S. Dolezal, I. Farrenkothen, and K. Mutter (1996), CFCs: Natural background emission by volcanoes?, *Eos Trans. AGU*, *77*(46), Fall Meet. Suppl., F804.

Wahrenberger, C., T. M. Seward, and V. Dietrich (1998), Halocarbon compounds in high temperature volcanic gases, paper presented at IAVCEI Congress, Int. Assoc. of Volcanol. and Chem. of the Earth's Inter., Cape Town, South Africa, July.

Wardell, L. J., P. R. Kyle, and C. Chaffin (1999), CO_2 emissions from Mount Erebus volcano, Antarctica, paper presented at 8th International Symposium on Antarctic Earth Science, R. Soc. of N. Z., Wellington.

Wilkniss, P. E., J. W. Swinnerton, R. A. Lamontagne, and D. J. Bressan (1975), Trichlorofluoromethane in troposphere, distribution and increase, 1971 to 1974, *Science*, *187*, 832–834.

Zolotov, M. Y., and E. L. Shock (2000), A thermodynamic assessment of the potential synthesis of condensed hydrocarbons during cooling and dilution of volcanic gases, *J. Geophys. Res.*, *105*(B1), 539–559.

V. J. Dietrich, F. M. Schwandner, and T. M. Seward, Institute of Mineralogy and Petrography (IMP), Swiss Federal Institute of Technology (ETH) Zürich, 8092 Zürich, Switzerland. (fschwandner@asu.edu)

A. P. Gize, Department of Geological Sciences, University of Manchester, Manchester M13 9PL, UK.

P. A. Hall, Hall Analytical Ltd., Milbrook Business Centre, Floats Road, Manchester M23 9YJ, UK.